AD-A138 854 FINE LINE ELECTROMIGRATION THE EFFECT OF CROSSED THERMAL GRADIENTS(U) HONEYWELL INC PLYMOUTH MN SOLID STATE ELECRRONICS DIV P G BRUSIUS SEP 83 1/1

UNCLASSIFIED RADC-TR-83-224 F30602-81-C-0227 F/G 20/12 NL

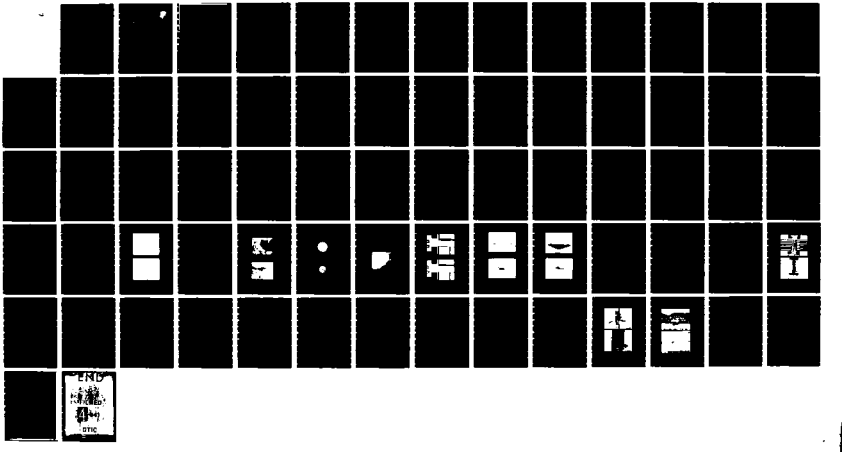

END

DTIC

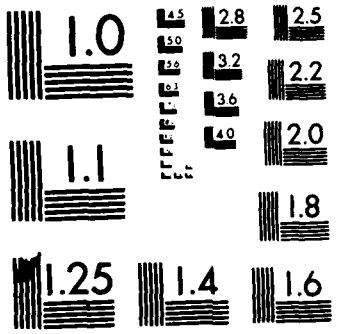

RADC-TR-83-224
Final Technical Report
September 1983

FINE LINE ELECTROMIGRATION
The Effect of Crossed Thermal Gradients

Honeywell Solid State Electronic Division

Phillip G. Brusius

ROME AIR DEVELOPMENT CENTER
Air Force Systems Command
Griffiss Air Force Base, NY 13441

This report has been reviewed by the RADC Public Affairs Office (PA) and is releasable to the National Technical Information Service (NTIS). At NTIS it will be releasable to the general public, including foreign nations.

RADC-TR-83-224 has been reviewed and is approved for publication.

APPROVED:

MARK. W. LEVI
Project Engineer

APPROVED:

W. S. TUTHILL, Colonel, USAF
Chief, Reliability & Compatibility Division

FOR THE COMMANDER:

CARLO P. CROCETTI
Chief, Plans Office

If your address has changed or if you wish to be removed from the RADC mailing list, or if the addressee is no longer employed by your organization, please notify RADC (RBRP) Griffiss AFB NY 13441. This will assist us in maintaining a current mailing list.

Do not return copies of this report unless contractual obligations or notices on a specific document requires that it be returned.

UNCLASSIFIED

SECURITY CLASSIFICATION OF THIS PAGE (When Data Entered)

REPORT DOCUMENTATION PAGE		READ INSTRUCTIONS BEFORE COMPLETING FORM
1. REPORT NUMBER RADC-TR-83-224	2. GOVT ACCESSION NO. AD-A138854	3. RECIPIENT'S CATALOG NUMBER
4. TITLE (and Subtitle) FINE LINE ELECTROMIGRATION The Effect of Crossed Thermal Gradients		5. TYPE OF REPORT & PERIOD COVERED Final Technical Report 1 Jul 81 - 30 Jun 83 6. PERFORMING ORG. REPORT NUMBER N/A
7. AUTHOR(s) Phillip G. Brusius		8. CONTRACT OR GRANT NUMBER(s) F30602-81-C-~~0027~~ 0217
9. PERFORMING ORGANIZATION NAME AND ADDRESS Honeywell Solid State Electronic Division 12001 State Highway 55 Plymouth NM 55441		10. PROGRAM ELEMENT, PROJECT, TASK AREA & WORK UNIT NUMBERS 61102F 2306J413
11. CONTROLLING OFFICE NAME AND ADDRESS Rome Air Development Center (RBRP) Griffiss AFB NY 13441		12. REPORT DATE September 1983 13. NUMBER OF PAGES 72
14. MONITORING AGENCY NAME & ADDRESS(if different from Controlling Office) Same		15. SECURITY CLASS. (of this report) UNCLASSIFIED 15a. DECLASSIFICATION/DOWNGRADING SCHEDULE N/A

16. DISTRIBUTION STATEMENT (of this Report)

Approved for public release; distribution unlimited.

17. DISTRIBUTION STATEMENT (of the abstract entered in Block 20, if different from Report)

Same

18. SUPPLEMENTARY NOTES

RADC Project Engineer: Mark W. Levi (RBRP)

19. KEY WORDS (Continue on reverse side if necessary and identify by block number)

Fine Line Electromigration
Thermal Gradient

20. ABSTRACT (Continue on reverse side if necessary and identify by block number)

The electromigration process is influenced by many microstructural and physical conditions. One condition that has not been studied is the effect of a thermal gradient perpendicular to the stripe length. This concern is especially interesting in the VLSI, near-micro line technology where the current density demands and uncertainties are growing.

DD FORM 1 JAN 73 1473 EDITION OF 1 NOV 65 IS OBSOLETE

UNCLASSIFIED

SECURITY CLASSIFICATION OF THIS PAGE (When Data Entered)

EVALUATION

This effort has provided technically useful information for one metallization system on the effect of heat flow across a small conductor subjected to a simultaneous electrical current. The results are not clear. Although a null hypothesis is satisfied statistically, there is a hint of a small effect. In hindsight, a better choice of metallization for detecting the effect would have been pure aluminum, rather than an aluminum alloy over a Ti-W barrier layer since the barrier layer must reduce the thermal gradients in the aluminum alloy, particularly at the critical corner locations. However, the establishment of no significant effect in an actually used metallization system is more than adequate compensation for the lack of sufficient information to extrapolate confidently to other metallizations.

MARK W. LEVI
Reliability Physics Section
Microelectronics Reliability Branch

TABLE OF CONTENTS

I.	INTRODUCTION	6
II.	THERMAL MODELING	8
III.	TEST STRUCTURE DESIGN AND FABRICATION	31
IV.	THERMAL CHARACTERIZATION	36
V.	PHYSICAL ANALYSIS	38
VI.	ELECTROMIGRATION LIFETIME TESTING	49
VII.	CONCLUSIONS AND RECOMMENDATIONS	63

LIST OF ILLUSTRATIONS

FIGURE NO.	TITLE	PAGE
II-1	SURFACE TEMPERATURES FROM POWERED JUNCTIONS	9
II-2	SILICON SURFACE TEMPERATURE	11
II-3	SILICON SURFACE GRADIENT	12
II-4	SILICON SURFACE TEMPERATURES FOR DIFFERENT SIZE JUNCTIONS	13
II-5	SILICON SURFACE GRADIENTS FOR TEMPERATURES SHOWN IN FIGURE II-4	14
II-6	SILICON TEMPERATURES AND GRADIENTS FOR JUNCTIONS 16 MICRONS APART	16
II-7	THERMAL GRADIENTS FOR 1.5 MICRON WIDE JUNCTION WITH 20 MICROWATTS	17
II-8	EFFECT OF SI GRADIENT ON CONDUCTOR TEMPERATURES	18
II-9	NORMALIZED TEMPERATURE DISTRIBUTION OF ALUMINUM STRIPE ON SILICON	19
II-10	EFFECT OF POWERED JUNCTION ON ABOVE STRIPE TEMPERATURE	21
II-11	GRADIENT IN 4 MICRON WIDE ALUMINUM CONDUCTOR OVER 2 MICRON WIDE JUNCTION	22
II-12	EFFECT OF POWERED JUNCTION ON ABOVE STRIPE TEMPERATURE	23
II-13	TEMPERATURE AND GRADIENT IN ALUMINUM CONDUCTOR AND SiO_2 ABOVE 10 MICRON JUNCTION HEATSOURCE	24
II-14	ALUMINUM CONDUCTOR LOCATED OVER EDGE OF POWERED JUNCTION	25

FIGURE NO.	TITLE	PAGE
II-15	GRADIENT VS JUNCTION DEPTH -- 1.5 MICRON^2 JUNCTION WITH 20μW POWER	26
II-16	GRADIENT FOR DIFFERENT JUNCTION DEPTHS 10 MICRON^2 JUNCTION WITH 3mW POWER	27
II-17	EFFECT OF POWERED JUNCTION ON ADJACENT STRIPE TEMPERATURE	29
II-18	TEMPERATURE AND GRADIENT ALONG HORIZONTAL PLANE OF CONDUCTOR OF FIGURE II-17	30
III-1	THERMAL GRADIENT TEST CHIP FEATURES	32
III-2	COMPLETE THERMAL TEST CHIP	33
V-1	OPTICAL PHOTOGRAPHS OF AS-DEPOSITED AL (0.5% CU) TEST PAD	39
V-2	TRANSMISSION ELECTRON PHOTOGRAPHS OF AS-DEPOSITED AL (0.5% CU) METALLIZATION	41
V-3	ELECTRON DIFFRACTION PATTERN FROM AS-DEPOSITED AL (0.5% CU)	42
V-4	TRANSMISSION ELECTRON PHOTOGRAPH OF AS-DEPOSITED AL (0.5% CU)	43
V-5	OPTICAL PHOTOGRAPHS OF 0.7 MICRON TEST PATTERN OF AL (0.5% CU)	44
V-6	SECONDARY ELECTRON PHOTOGRAPHS OF CROSS SECTION OF AN AS-DEPOSITED AL (0.5% CU) LINE WITH NOMINAL WIDTH OF 2.5 MICRONS	45
V-7	SECONDARY ELECTRON PHOTOGRAPHS OF CROSS SECTION OF AN AS-DEPOSITED AL (0.5% CU) TEST LINE WITH NOMINAL WIDTH OF 0.7 MICRONS	46
V-8	AUGER ELECTRON SPECTROSCOPY SURVEY OF SPUTTER ION CLEANED AL (0.5% CU) BONDING PAD	47

FIGURE NO.	TITLE	PAGE
V-9	AUGER DEPTH PROFILE OF AS-DEPOSITED AL (0.5% CU)	48
V-10	NORMAL AND EBIC IMAGES OF TEST DEVICE	50
VI-1	RESISTANCE VERSUS TIME PLOT OF DEVICE IN FIRST TEST	54
VI-2	RESISTANCE VERSUS TIME PLOT OF DEVICE IN SECOND TEST	56
VI-3	TEMPERATURE CORRECTED RESISTANCE VERSUS TIME PLOT OF SAME DEVICE	57
VI-4	SEM PICTURES OF DEFECTS IN 5 MICRON LINES CAUSED BY STRESS TEST	61
VI-5	SEM PICTURES OF DEFECTS IN 5 MICRON LINES CAUSED BY STRESS TESTS	62

LIST OF TABLES

TABLE NO.	TITLE	PAGE
II-1	TEMPERATURE/GRADIENT RANGE	15
III-1	TEST PATTERN VARIATION	35
III-2	AVAILABLE DICE PER TEST PATTERN	36
IV-1	DIODE TEMPERATURES FOR DIFFERENT HEATING CURRENTS	37
VI-1	TEST 1: RESISTANCE, TEMPERATURE, AND TIME TO FAIL DATA	52
VI-2	TEST 2: RESISTANCE, TEMPERATURE, AND TIME TO FAIL DATA	55
VI-3	TEST 2 SUMMARY	58
VI-4	TEST 3: RESISTANCE, TEMPERATURE, AND TIME TO FAIL DATA	59
VI-5	TEST 3 SUMMARY	60

I. INTRODUCTION

Electromigration is the phenomenon where current flow in conductors causes a momentum exchange which can, under certain conditions, result in mass transport in the conductor. Conducting material accumulates in some places on a line; voids are also created. In integrated circuits, this mechanism manifests itself in the form of high resistance lines, open circuits and/or whisker growth, which can lead to failures. Screening for the defects which cause electromigration is time consuming, difficult, and inappropriate for VLSI.

While the factors contributing to electromigration in 5μm IC geometries are reasonably well understood, there is an uncertainty in evaluating VLSI electromigration reliability because of the potential lack of applicability of simple stripe test data to actual VLSI microcircuits. For example, thermal gradients may exist throughout integrated circuits due to many current-carrying gates crowded in one area, topological or geometrical changes in oxides and conductors, interconnect metal heat sinks in the die middle, or die bond voids of varying sizes. While actual temperature variations are relatively small, gradients may be large. The gradients may be in all directions and they may be time varying. The effect of such gradients on narrow line electromigration is not clear.

Thermal gradients are known to affect macro electromigration. In tests where gradients were parallel to the test stripes, Black[1] observed void formation on positive gradients and hillock formation on negative gradients. This condition results from the fact that the mass transport is in the direction of electron flow and is activated by temperature.

1 J. R. Black, "Electromigration - A Brief Survey and Some Recent Results," IEEE Transactions on Electron Devices, ED-16, 1969, pp. 338-347.

The question of how crossed thermal gradients affect microcircuit electromigration has not been addressed. Because alloy developments have minimized electromigration problems on SSI and MSI, the above question has not needed answering. LSI and VLSI designs which call for higher current densities now make the thermal gradient problem very meaningful.

This study examines the effect of crossed thermal gradient on electromigration. Section II reports some thermal modeling of silicon structures that estimated possible gradients. The next section, describes a specially designed test vehicle that features an implanted resistor heat source which produces a crossed thermal gradient on electromigration test stripes. Sections IV and V discuss the thermal and physical characterization of the test samples. Section VI details the results of accelerated tests which compared lifetimes of test stripes experiencing a realistic crossed thermal gradient with life-times of controls.

II. THERMAL MODELING

In order to understand the types of temperatures and thermal gradients that might be present in silicon integrated circuits, thermal models were generated on a computer for various conditions. The computer modeling used finite element analysis and assumed different types of two dimensional test structures. This work was performed to analyze VLSI sized circuits for likely gradients and to analyze test structures that might be used to simulate these circuits. Relatively simple configurations were used, so as to allow the use of available computer programs. The results, however, should generally be applicable to more real structures. No appropriate results were available in the literature from which to draw.

Initially, four cases were analyzed to determine:

1. The effect of a powered junction on the silicon surface temperature:
2. The effect of a silicon thermal gradient on an aluminum conductor temperature and gradient;
3. The effect of a powered junction on an above aluminum conductor temperature and gradient;
4. The effect of a powered source on a nearby aluminum conductor temperature and gradient.

CASE I: THE EFFECT OF A POWERED JUNCTION ON THE SILICON SURFACE TEMPERATURE

The model shown in Figure II-1 was used for this work. Note that the silicon and the junction have a mirror image on the other side of the center line and extend to infinity in the plane perpendicular to the paper. Thus, in this example, the junction is 2w wide and infinitely long. The purpose of this modeling was to determine which variables affected silicon thermal gradients significantly and to determine which model was appropriate to use.

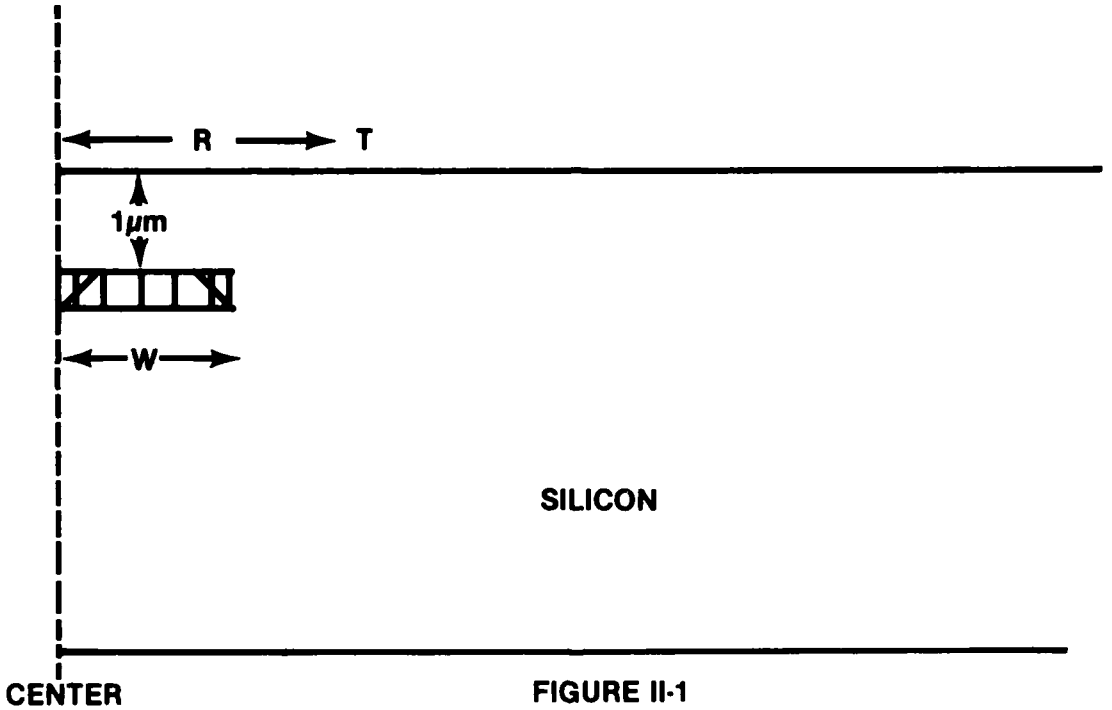

FIGURE II-1
SURFACE TEMPERATURES FROM POWERED JUNCTIONS

The finite element model (1) divides the cross section (e.g. Figure II-1 into a number of small rectangles of the appropriate material, (2) assigns temperastures to the source rectangles, and (3) calculates temperatures for the other rectangles using the known physical constants and distances. The physical values used were taken to be constant and not temperature dependent. Specific thermal conductivities used were: SiO_2 - .014 w/cm°C, aluminum - 2.0 w/cm°C, silicon 1.1 w/cm°C, and air.0003 w/cm°c. The sizes of the rectangles throughout the cross section were judiciously chosen so as to best depict the temperatures of the area of interest. For example, the rectangles were small around the junction and much larger at the right side of Figure II-1. The analysis was generally carried out with about 25 vertical layers, each divided into 25 horizontal pieces, i.e., around 625 elements (rectangles).

For ease of comparison, the heat source was powered such that the junction "temperature" was 1000°C. The computer program ran more smoothly if only 1 rectangle was at 1000°C. Figure II-2 shows temperatures across the top of the silicon for 3 cases:

1) Where the 1000°C rectangle is at the centerline;

2) Where the 1000°C rectangle is at the junction periphery;

3) Where the whole junction is 1000°C.

Figure II-3 shows the gradients for the top rectangles of the silicon for these three cases. These graphs indicate that the gradient is not significantly different for the 3 cases and that the peak gradient is right above the outside of the junction. Figures II-4 and II-5 show the temperatures and gradients respectively for different size junctions. Although different power levels were required in each case, Figure II-5 demonstrates that, if the junction temperature is fixed, smaller junctions produce higher thermal gradients.

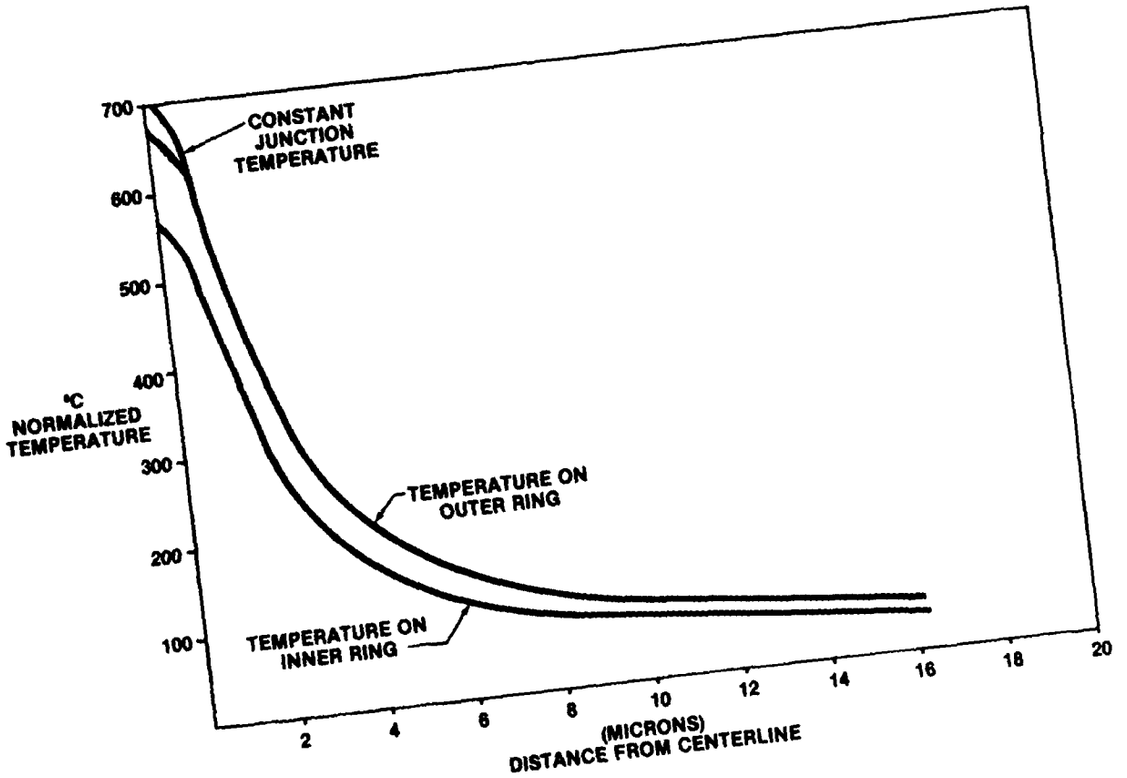

FIGURE II-2
SILICON SURFACE TEMPERATURE
1.5 MICRON WIDE JUNCTION

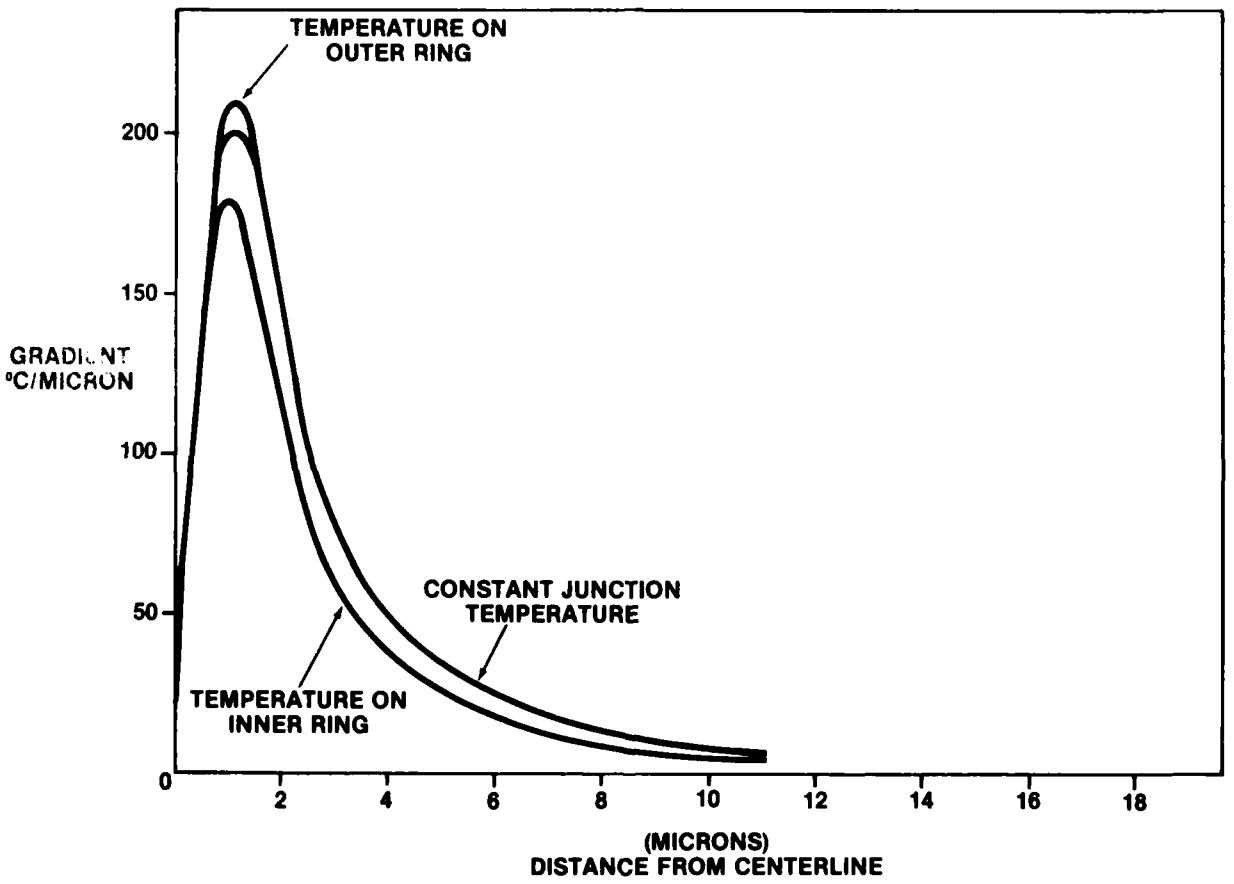

FIGURE II-3
SILICON SURFACE GRADIENT
FOR CASE SHOWN IN FIGURE II-2

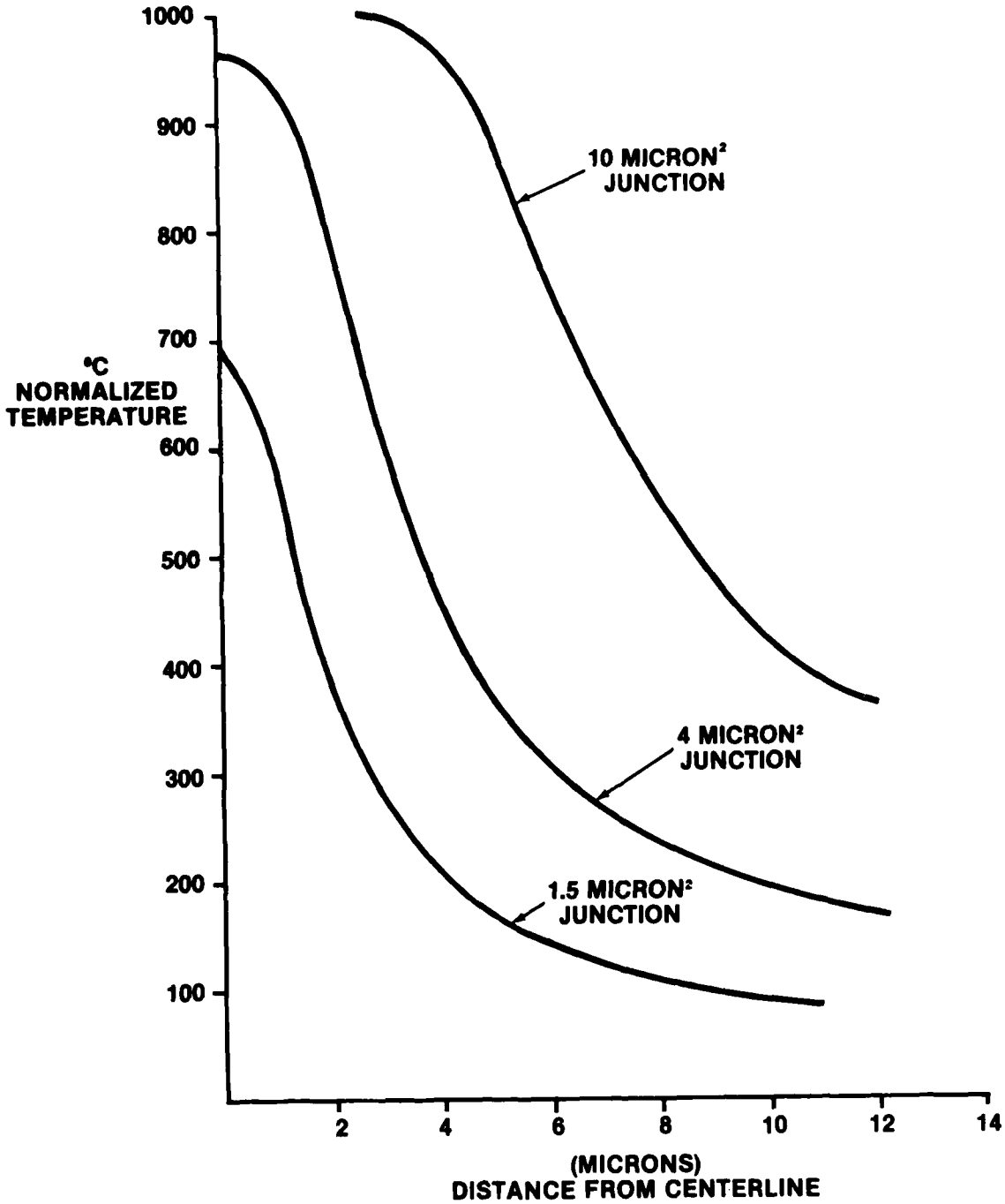

FIGURE II-4
SILICON SURFACE TEMPERATURES
FOR DIFFERENT SIZE JUNCTIONS

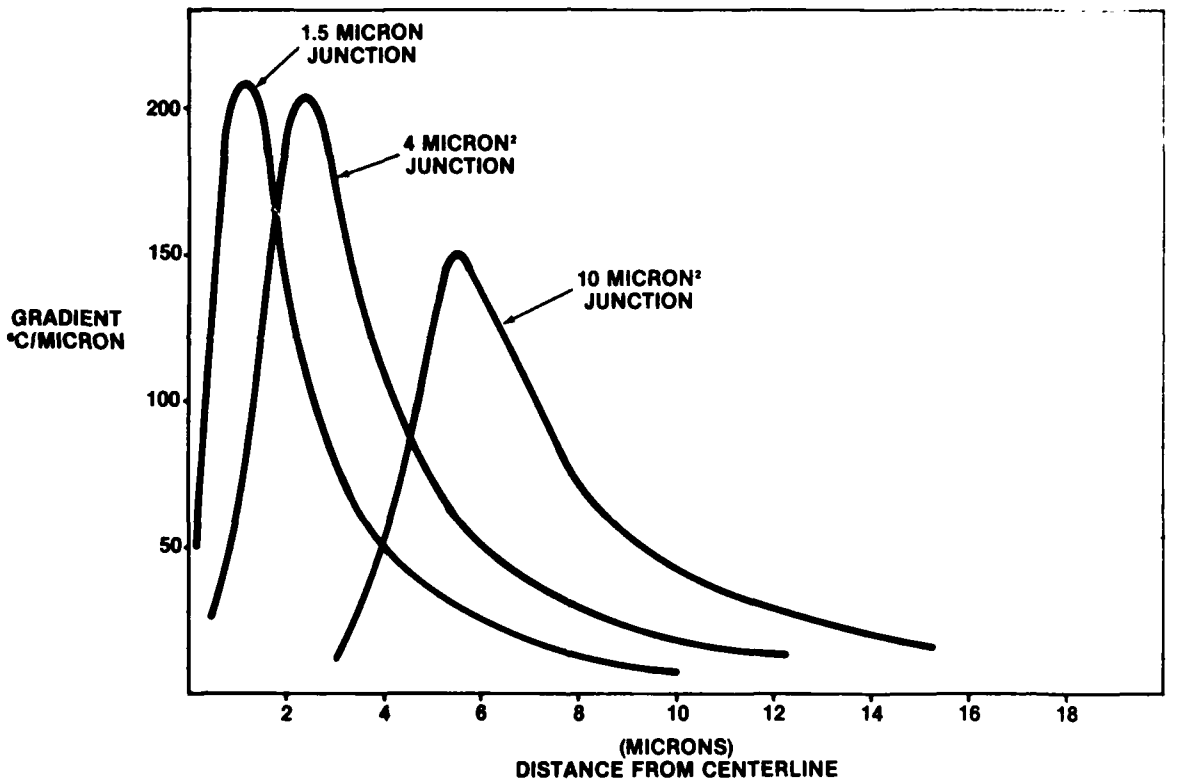

FIGURE II-5
SILICON SURFACE GRADIENTS FOR
TEMPERATURES SHOWN IN FIGURE II-4

The above discussion was based on a single junction on a large silicon die. To approximate the real case where a number of junctions exist on a single die, consider a 200 mil^2 chip with 100,000 junctions. If these junctions are equally spaced, then they will be on a grid such that each junction is 16 microns from its 4 nearest neighbors. For computational purposes, each junction is on a die that is 16 microns square. The temperatures and gradients associated with such a structure are shown in Figure II-6. Again it is noted that smaller junctions have the larger gradients.

If the above example is adjusted to dissipate 20 microwatts in the junction and is compared with a similarly adjusted case where there is one junction on a large die, the graph of Figure II-7 results. Thus, the junction spacing is not a significant factor. The same situation exists for a 3 milliwatt, 10 micron square junction. These results are summarized in Table II-1 which shows the type of surface gradients that might exist in a powered silicon device.

TABLE II-1
T E M P E R A T U R E / GRADIENT
R A N G E

		POWER/JUNCTION	
		20μ Watts/1.5μm^2	3m Watt/10μm^2
TEMP RISE ABOVE AMBIENT	1 Device/Chip	.015°C	.845°C
	10^5 Devices/Chip	.147°C	20.5°C
GRAD	1 Device/Chip	.005°C/μ	.112°C/μ
	10^5 Device/Chip	.005°C/μ	.089°C/μ

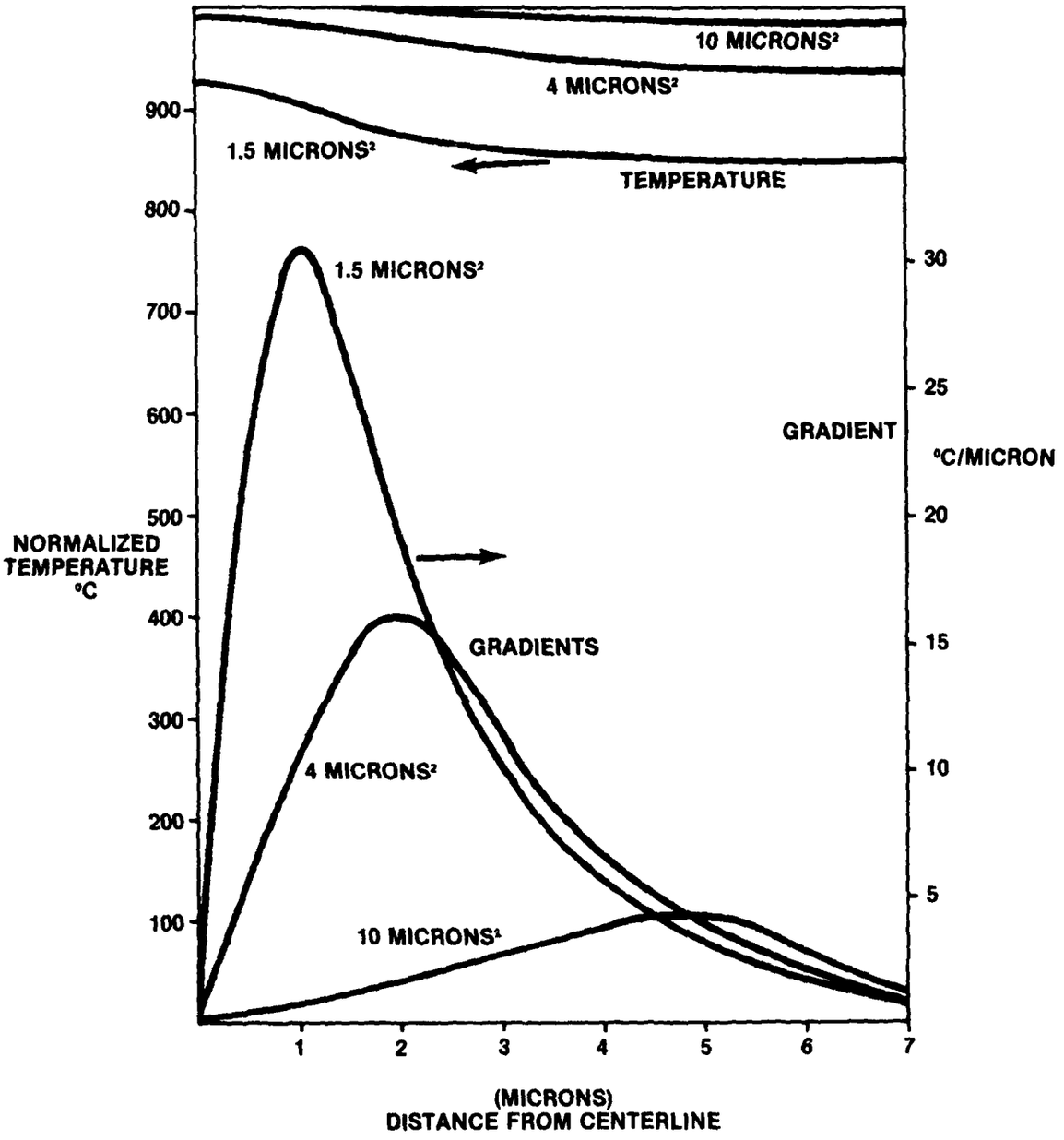

FIGURE II-6
SILICON TEMPERATURES AND GRADIENTS FOR JUNCTIONS 16 MICRONS APART

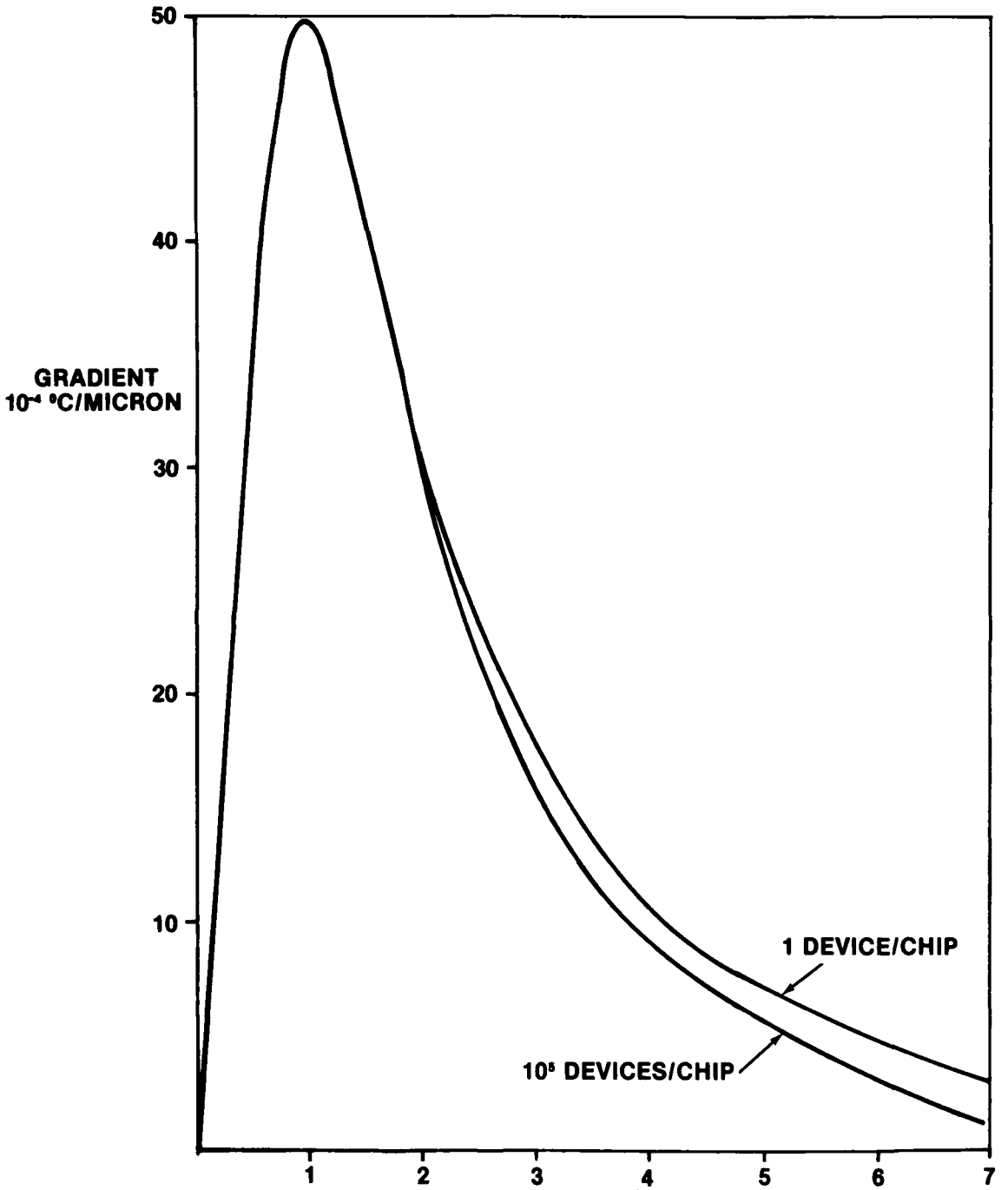

FIGURE II-7
THERMAL GRADIENTS FOR 1.5 MICRON WIDE JUNCTION WITH 20 MICROWATTS

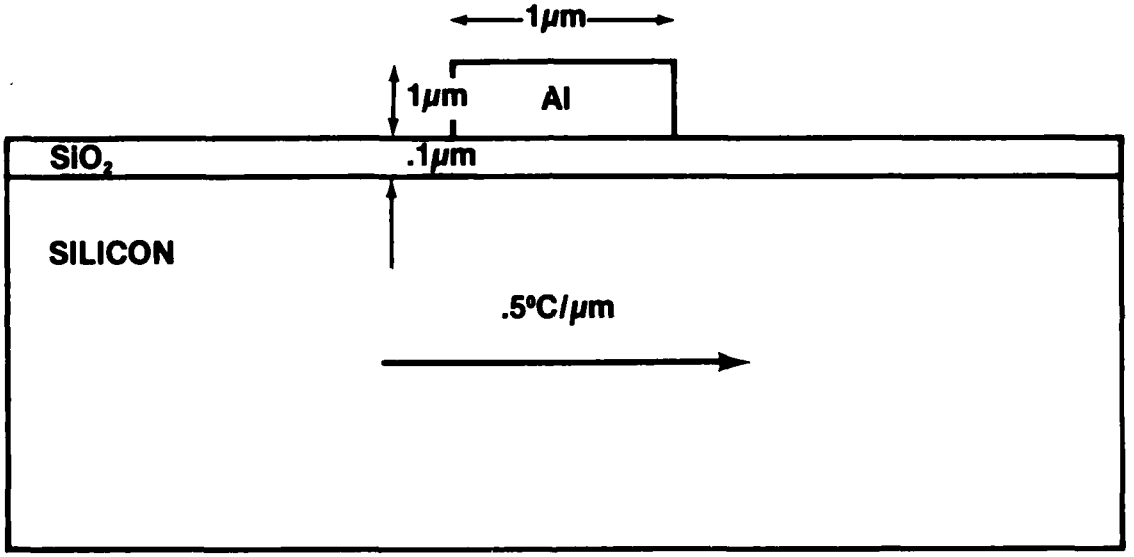

FIGURE II-8
EFFECT OF SI GRADIENT
ON CONDUCTOR TEMPERATURE

CASE II: THE EFFECT OF A SILICON GRADIENT ON A CONDUCTOR TEMPERATURE

The model for this case is shown in Figure II-8. The results of the computer simulation with an assumed gradient in the silicon of .5°C/micron are shown in Figure II-9. Gradients are difficult to estimate from this data because of the temperature non-linearity at the aluminum - SiO_2 interface. With the exception of the extreme outer edges of the aluminum, the thermal gradients are generally less than .01°C/micron. Thus, there is a reduction of some 50x, and the aluminum stripe effectively shorts out the silicon gradient.

FIGURE II-9

NORMALIZED TEMPERATURE DISTRIBUTION OF 1 µm X 1 µm ALUMINUM STRIPE ON SILICON CARRYING .5°C/µm THERMAL GRADIENT

	-.173	-.108	-.040	-.013	0	+.013	+.040	+.108	+.173
1µm	-.157	-.002	-.002	-.001	0	+.001	+.002	+.002	+.157
	-.153	-.002	-.002	-.001	0	+.001	+.002	+.002	+.153
	-.158	-.002	-.002	-.001	0	+.001	+.002	+.002	+.158
	-.170	-.003	-.002	-.001	0	+.001	+.002	+.003	+.170
	-.192	-.004	-.003	-.002	0	+.002	+.003	+.004	+.192
	-.235	-.005	-.004	-.002	0	+.002	+.004	+.005	+.235
	-.337	-.008	-.005	-.003	0	+.003	+.005	+.008	+.337
	-.328	-.243	-.160	-.080	0	+.080	+160	+.243	+.328
	-.329	-.246	-.164	-.082	0	+.082	+.164	+.246	+.329

AIR

SILICON

1µ

(°C)

CASE III: THE EFFECT OF A POWERED JUNCTION ON AN ABOVE ALUMINUM CONDUCTOR TEMPERATURE AND GRADIENT

Figure II-10 depicts the configuration simulated for this case. The results of the modeling are graphed in Figure II-11. As noted earlier, the thermal gradient in the aluminum is generally modest except for a sharp rise at its edge. A variation of this situation is shown in Figure II-12. Here the aluminum conductor is essentially an infinite plane over an infinitely long junction of finite width. The results of the simulation show that the gradient is relatively smooth across the conductor.

This case was also examined for a 10 micron wide junction. The computed temperature and gradient profile are shown in Figure II-13. This graph also shows the temperature and gradient that would exist in the SiO_2 if the aluminum were not present. Thus, in instances where a large sheet of aluminum passes over a powered junction, a significant amount of the silicon gradient remains in the aluminum. However, this is essentially a longitudinal gradient and not directly applicable to the crossed thermal gradient of interest here.

Another useful variation of this case exists when the aluminum conducting stripe is centered over the edge of the junction. This case is depicted in Figure II-14. The gradients in the silicon have been calculated for this situation with different junction widths. Specific power levels have been applied: 20 microwatts for a 1.5 micron wide junction and 3 milliwatts for a 10 micron wide junction. The results are shown in Figure II-15 and II-16.

The above results indicate silicon and SiO_2 gradients greater than 0.2°C/micron exist in VLSI circuits. It was noted earlier (Case II) that the high thermal conductivity of the aluminum tended to short out the silicon gradient. The degree of this shorting effect depends upon the relative thermal conductivities (i.e., the thermal conductivity of aluminum is about

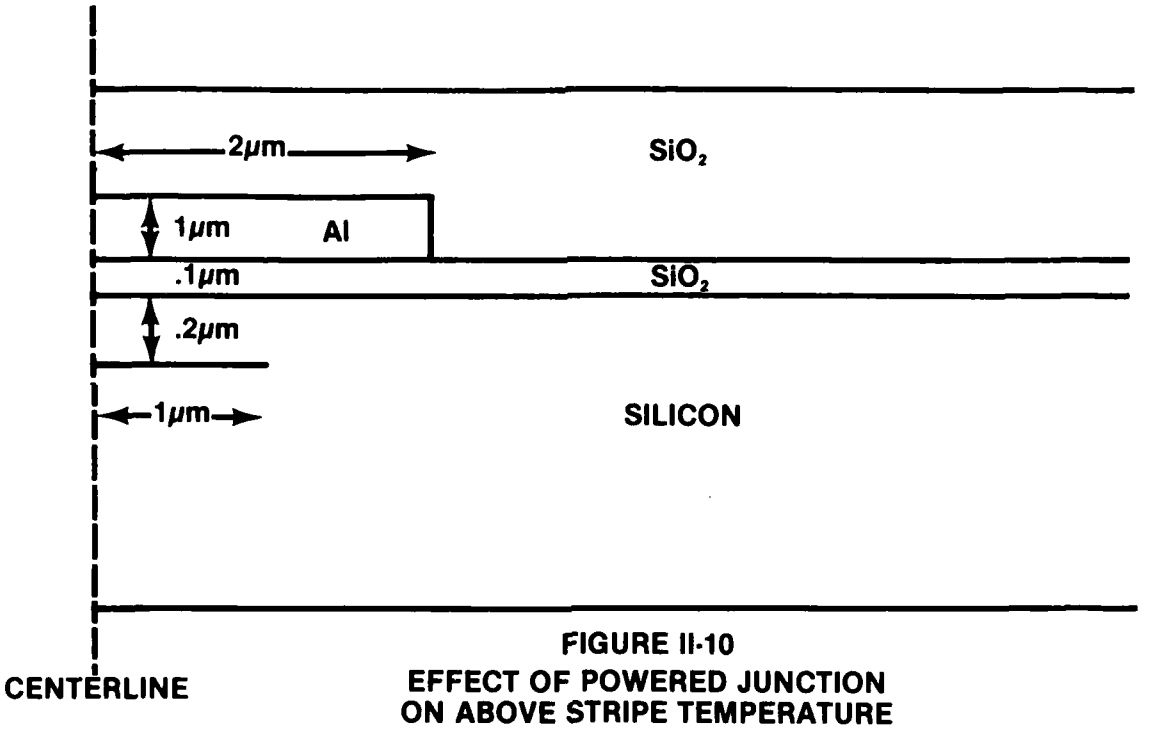

FIGURE II-10
EFFECT OF POWERED JUNCTION ON ABOVE STRIPE TEMPERATURE

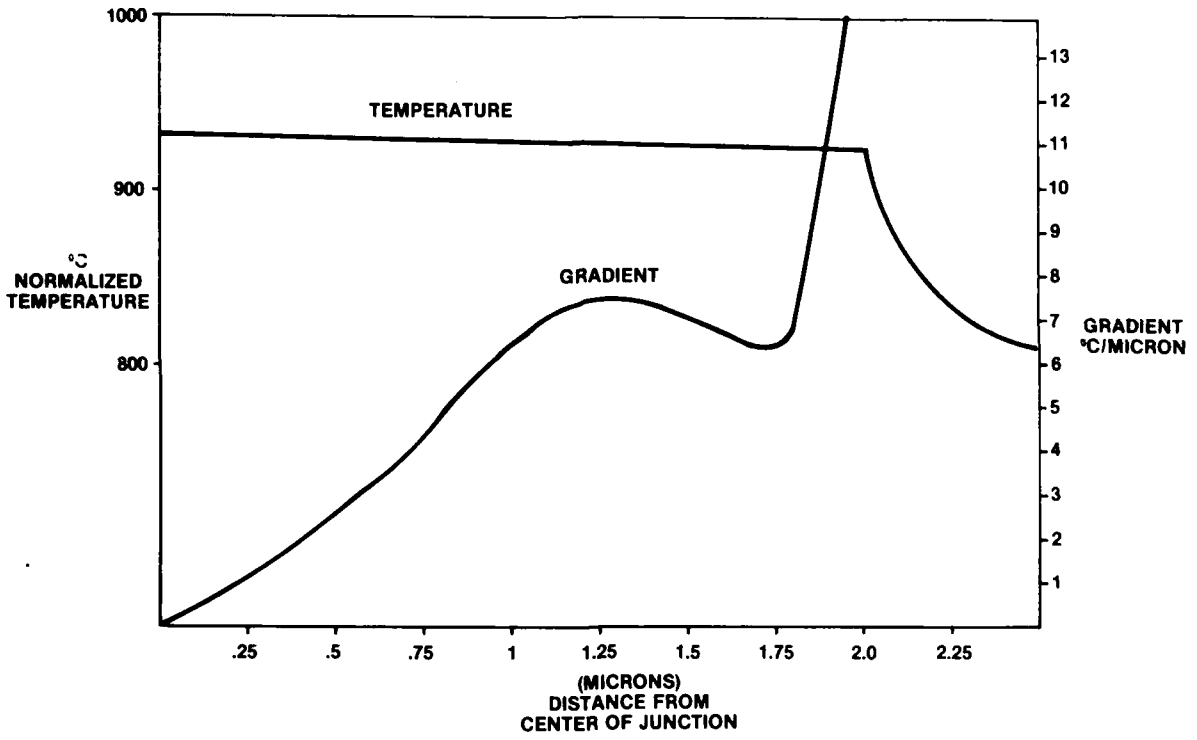

FIGURE II-11
GRADIENT IN 4 MICRON WIDE ALUMINUM
CONDUCTOR OVER 2 MICRON WIDE JUNCTION

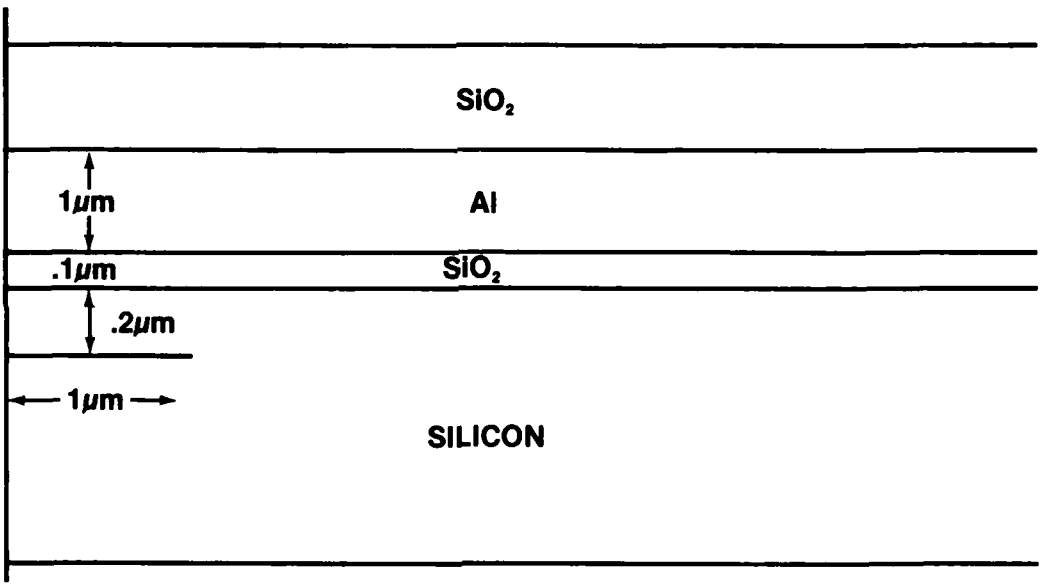

FIGURE II-12
EFFECT OF POWERED JUNCTION ON ABOVE STRIPE TEMPERATURE

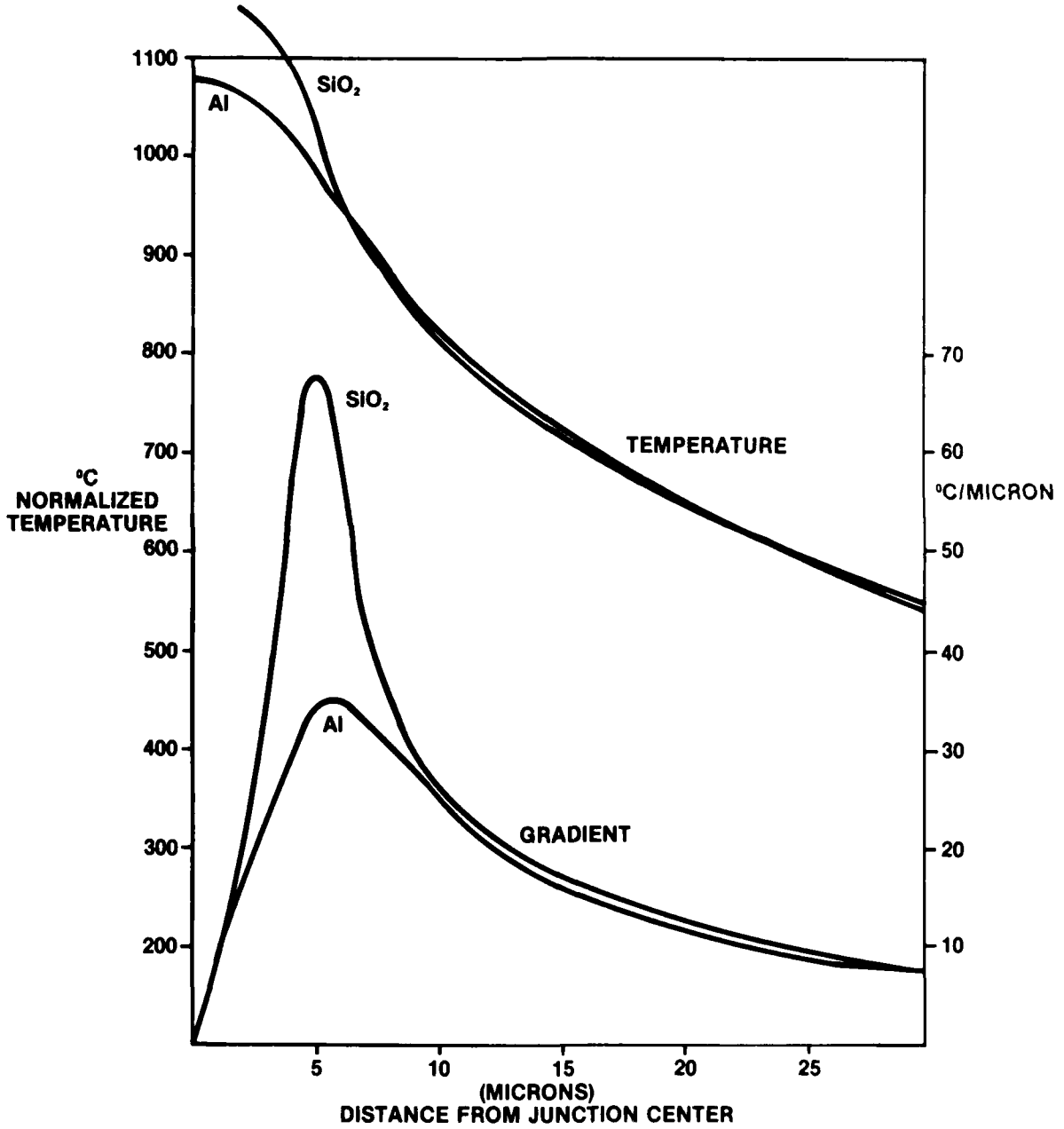

FIGURE II-13
TEMPERATURE AND GRADIENT IN ALUMINUM CONDUCTOR AND SiO_2 ABOVE A 10 MICRON JUNCTION HEATSOURCE

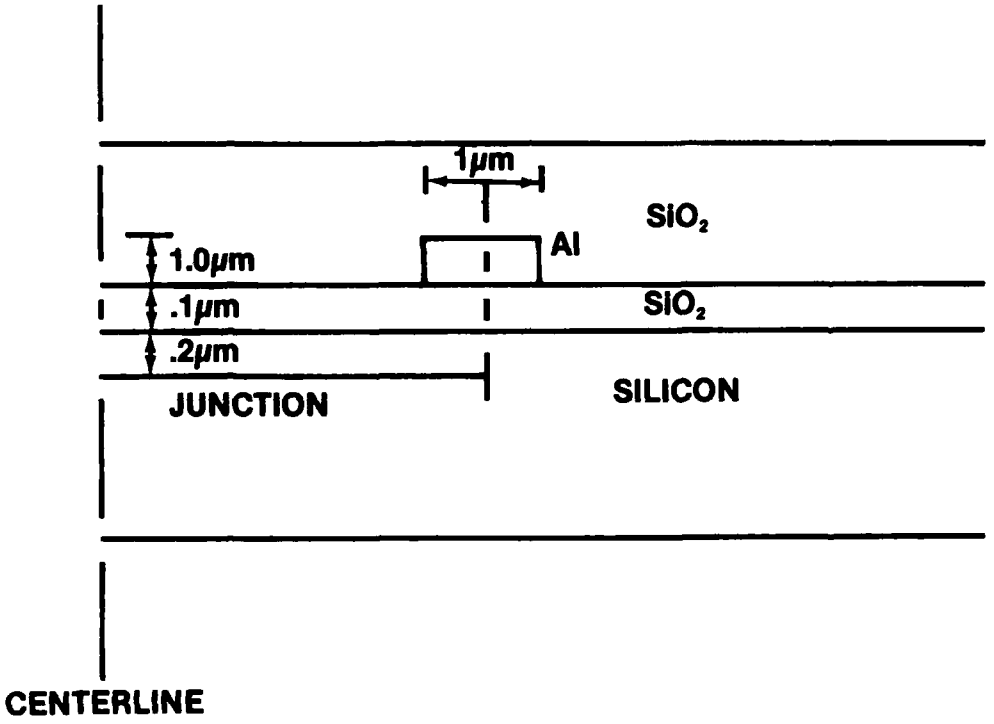

FIGURE II-14
ALUMINUM CONDUCTOR LOCATED OVER EDGE OF POWERED JUNCTION

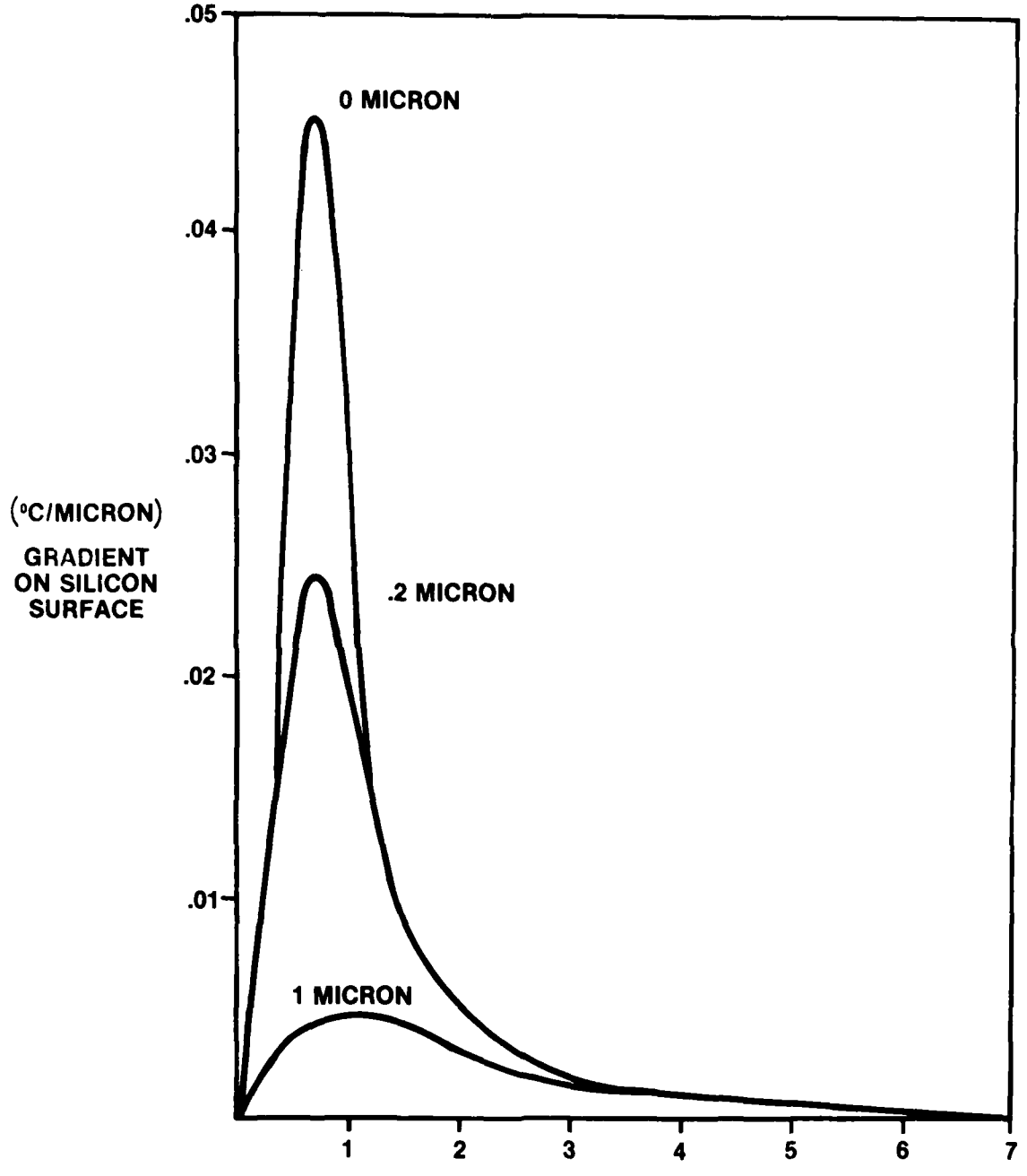

FIGURE II-15
GRADIENT vs JUNCTION DEPTH
1.5 MICRON JUNCTION WITH 20μW POWER

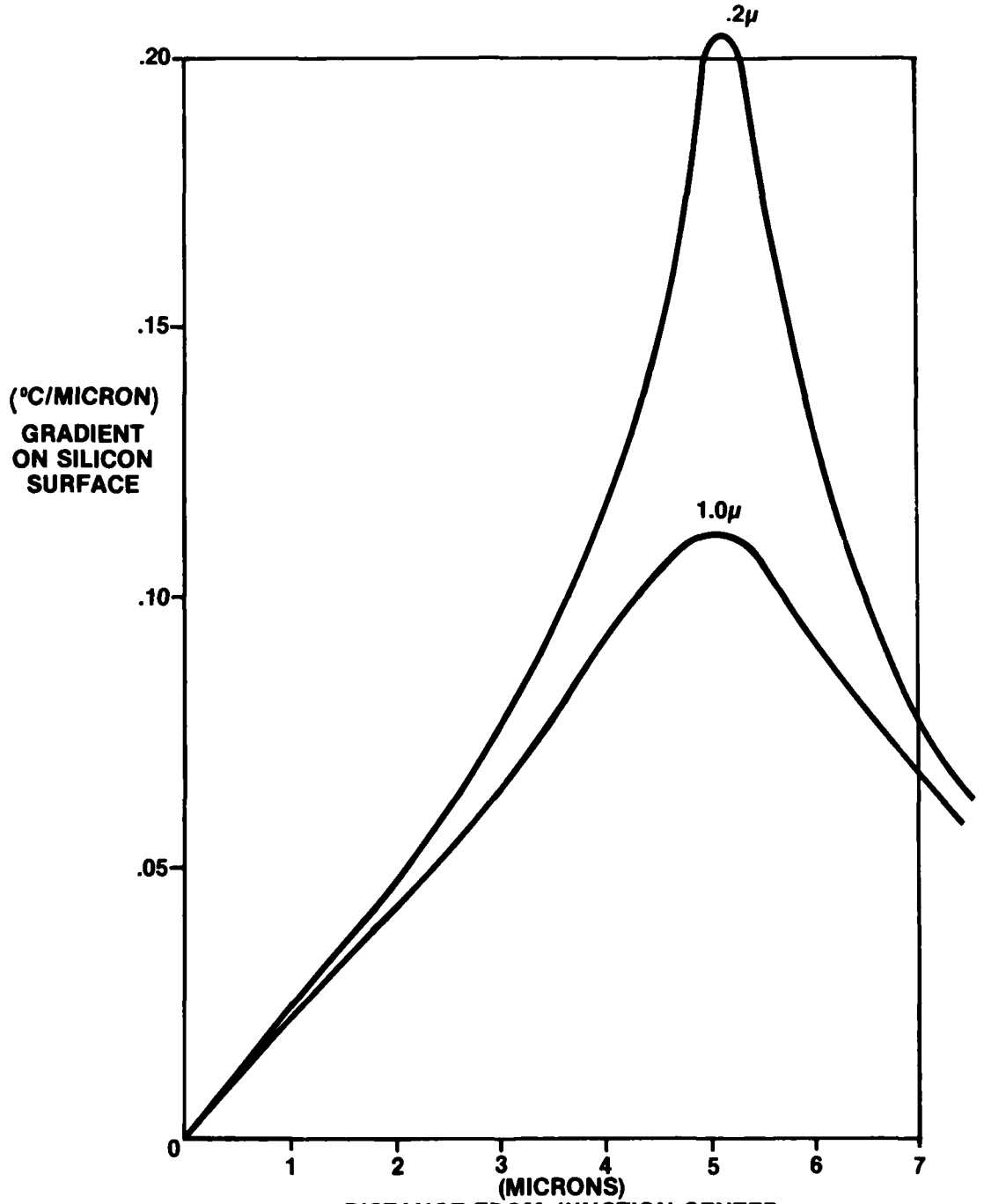

FIGURE II-16

GRADIENT FOR DIFFERENT JUNCTION DEPTHS 10 MICRON² JUNCTION 3mW POWER

70 X that of SiO_2) and the specific geometries (important items are aluminum cross sectional area and the amount and type of material covering the aluminum on the top and 2 sides). In Case II, the aluminum line (1 micron x 1 micron line surrounded by air) carried 1/50 the silicon gradient. Additional modeling showed that a wider aluminum line (3 microns wide by .5 micron thick), surrounded by SiO_2, would hold 1/10 the silicon gradient. Also, a 1 micron wide by .5 micron thick aluminum line, surrounded by SiO_2, maintains about 1/40 the silicon gradient.

Thus, crossed thermal gradients around .02°C/micron exist in the aluminum. Also, the aluminum gradient is greater for a 3 micron line than for a 1 micron line. This is true because some heat enters the aluminum from the top thru the SiO_2 and the wider line has more top surface from which more heat can enter.

CASE IV: THE EFFECT OF A POWERED HEAT SOURCE ON AN ADJACENT STRIPE TEMPERATURE

This case is similar to the previous one except that here the conductor stripe is some microns horizontally distant from the power source, as shown in Figure II-17. The results in Figure II-18 suggest that the aluminum conductor effectively shorts out the gradient that exists in the silicon. A similar situation was shown to exist if the heat source was an aluminum conductor in the same plane as the gradient conductor.

SUMMARY OF THERMAL MODELING RESULTS

Typical VLSI sized integrated circuits were thermally modeled on a computer using finite element analysis. Significant results are listed below.

1) Peak temperatures and gradients on a IC surface, both in the silicon and in the aluminum conductor, exist over the edge of a powered junction.

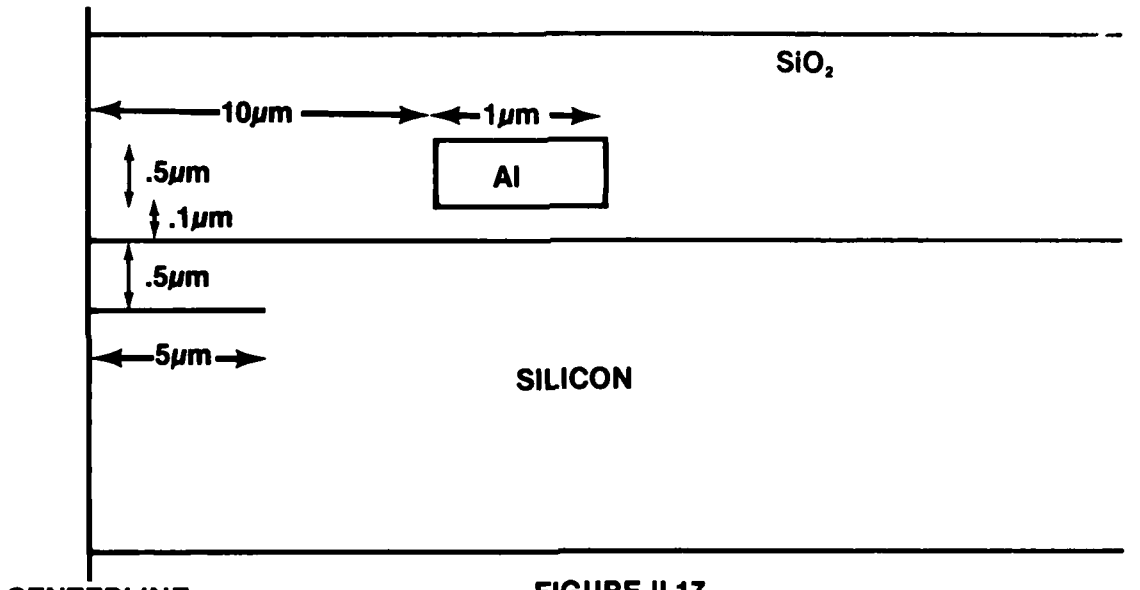

FIGURE II-17
EFFECT OF POWERED JUNCTION ON ADJACENT STRIPE TEMPERATURE

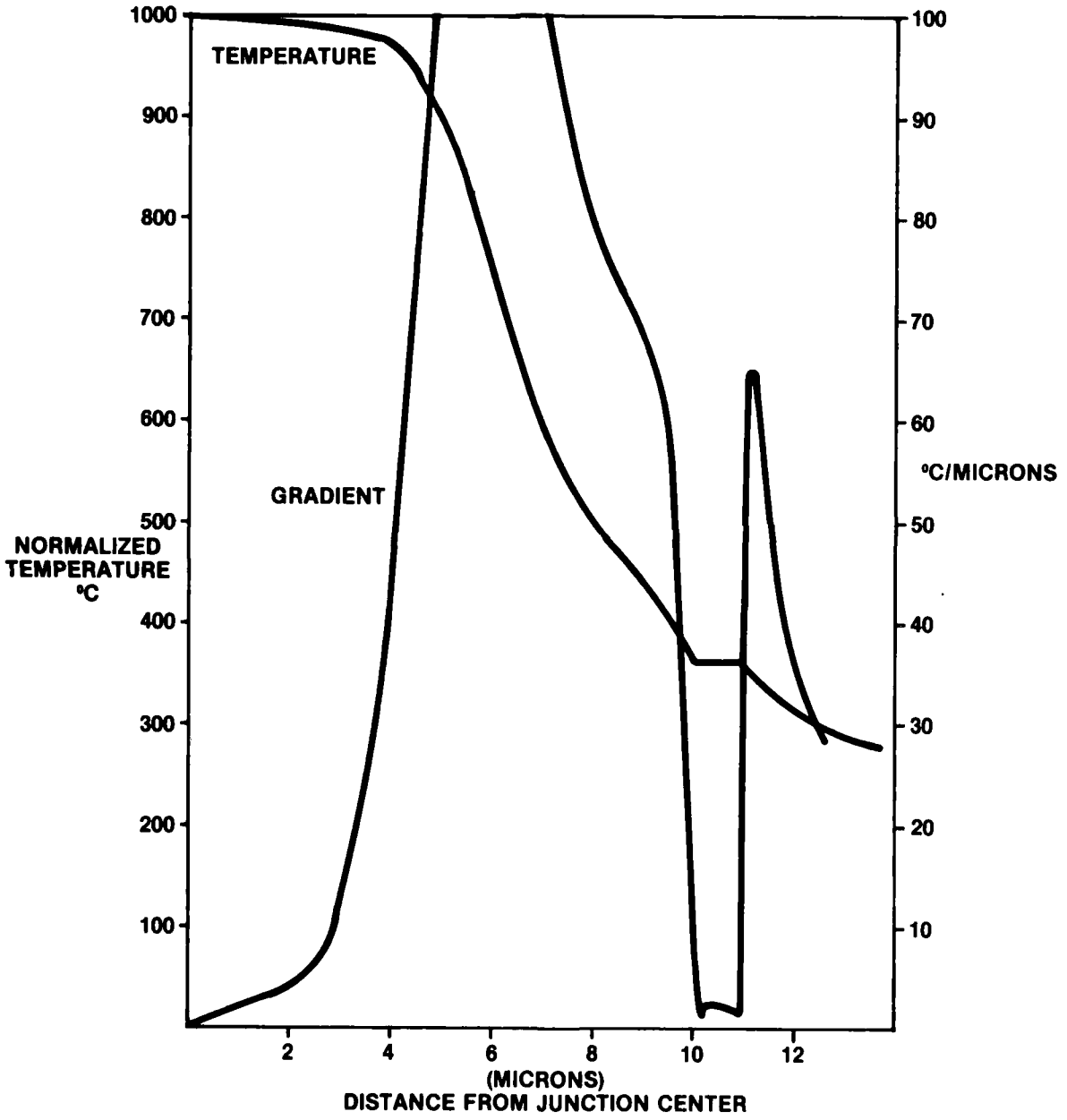

FIGURE II-18
TEMPERATURE AND GRADIENT ALONG HORIZONTAL PLANE OF CONDUCTOR OF FIGURE II-17

2) The aluminum conductor will short out (i.e., greatly reduce) a smooth gradient in the silicon. However, it will assume a significant portion (as much as half) of a sharp gradient in the silicon.

3) Thermal gradients greater than .1°C/micron exist in aluminum conductors in VLSI circuits.

III. TEST STRUCTURE DESIGN AND FABRICATION

The modeling in the previous chapter indicated that thermal gradients in the order of .02°C/micron will exist perpendicular to aluminum conductors on
VLSI circuits. The following text describes a test structure that was designed for an electromigration test to compare lifetimes of conductors with and without thermal gradients.

The basic test structure consists of a long straight, electromigration test line that is parallel to, and over the edge of a diffused resistor. The resistor creates a thermal gradient that is perpendicular to the long direction of the test line. An identical line is placed parallel to and over the center of the resistor to act as a control. Other structures were added to measure surface temperatures.

One of the test structures is shown in Figure III-1. Features of this test structure are described below. The entire chip is shown in Figure III-2.

1. The test structure has 2 test stripes: one in the middle of the diffused resistor to serve as a control, and one on the edge of the resistor to experience the gradient. Only one stripe on a given chip will be operated at high current density.

2. There are two means for measuring chip temperature: (a) three diodes are located at different distances from the diffused resistor; (b)

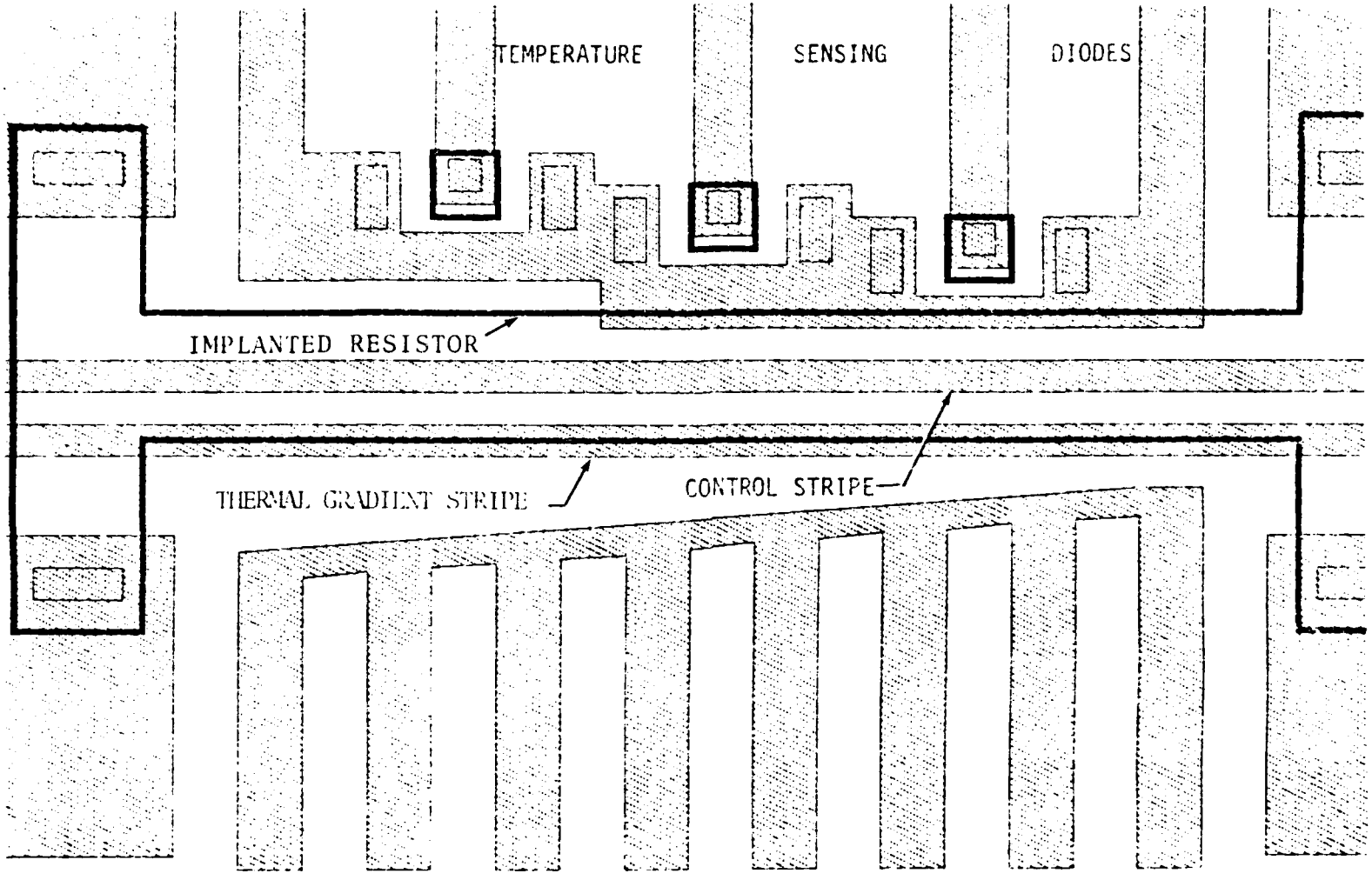

FIGURE III-1

THERMAL GRADIENT TEST CHIP FEATURES

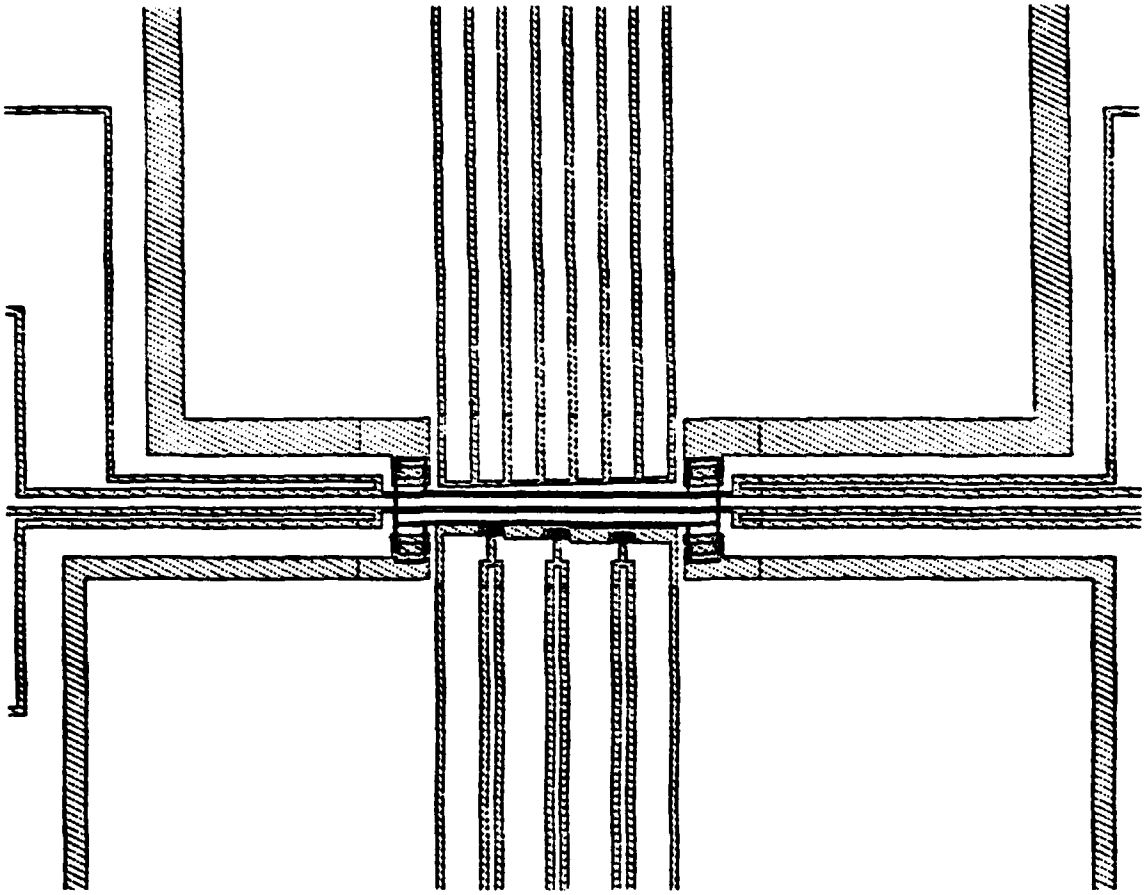

FIGURE III-2
COMPLETE THERMAL TEST CHIP

short lengths of conductors are similarly located on the other side of the diffused resistor. Both methods can be tried experimentally.

3. All lines/devices which might indicate temperature have Kelvin pads for improved accuracy.

4. The diffused resistor has four contacts - 2 on each side of the gradient test stripe. Using different sets of pads might be useful in sorting out electromigration problems that may occur at the end of the test stripe.

All photolithography work for this chip was be done on a Cambridge Instrument EBMF-6 direct-write E-beam system. Using the direct-write system has a number of advantages. Since conventional glass plate masks are not required, pattern changes could be made relatively easily through software. There is also the capability of using different test patterns with a single wafer or group of wafers. The total test pattern contains 9 distinct test patterns: three different sized resistors with each of three test line widths (nominally 0.7, 2.5, and 5 microns). Thus, a wafer could include all 9 different patterns or a regular stepping of a subset of the 9 patterns.

The wafer processing steps and the important characteristics of each are listed below. The starting materials was a p-type substrate (100) at 10 ohm-cm.

1. Buried Layer Poly Deposition (40 ohms/sq., 25 microns thick)
2. Buried Layer One Step Oxidation
3. Epi Deposition (1.2 microns thick, 0.7 ohm-cm)
4. 800 A Oxide Deposition
5. E-Beam Etch Pits
6. Oxide Etch
7. KOH Etch
8. Strip Oxide
9. Screening Oxide Deposition

10. E-Beam Inactive Base Cut
11. Inactive Base Implant (Boron, 2 X $10^{15}/cm^2$, 85 kev)
12. Anneal (900°C, 30 minutes H_2)
13. E-Beam Contact Cut
14. Contact Etch
15. Palladium Deposition/Vacuum Anneal (500Å)
16. Silicide Etch/Inspection
17. TiW Deposition (1200Å)
18. 1st Metal Deposition (5000Å, Aluminum 1% Copper)
19. E-Beam 1st Metal Cut (using polystrene resist and 2000Å Plasma Oxide Mask)
20. Anneal (450°C for 30 minutes).

There were a number of problems in the processing cycle, especially trying to set up a process to etch submicron lines. In the end 4 wafers had reasonably good test sites. The nine chip variations are listed in Table III-1 and the number of available dice on each are shown in Table III-2.

TABLE III-1
TEST PATTERN VARIATION

#	Resistor Size (Microns)	Test Stripe Width (microns)
1	20 x 180	5.0
2	20 x 180	2.5
3	20 x 180	0.7
4	40 x 360	5.0
5	40 x 360	2.5
6	40 x 360	0.7
7	40 x 720	5.0
8	40 x 720	2.5
9	40 x 720	0.7

TABLE III-2

AVAILABLE DICE PER TEST PATTERN

#	Wafer 20	Wafer 12	Wafer 14	Wafer 15
1	24	24		
2	24	24	24	24
3			24	24
4	24	24		
5	24	24	24	24
6			24	24
7	24	24		
8	24	24	24	24
9			24	24

For testing purposes, some 300 dice were packaged in 16 pin ceramic DIPS using standard packaging procedures.

IV. THERMAL CHARACTERIZATION

This section of the report describes the work that was done to measure the thermal gradients on the test patterns. Diodes and conductors were designed into the layout to act as temperature sensors. Conditions were varied so as to find a condition in which at least .1°C/micron would be applied perpendicular to the electromigration test stripe.

The surface temperature was characterized by calibrating the diodes over the expected temperature range, running various heating currents thru the diffused resistor, and sensing the corresponding surface temperature at the diodes. The diodes were calibrated by measuring the forward voltage drop at a specific current at temperatures of 25, 50, 75, 100, 125, and 150°C. Assuming the temperature and the voltage were linearly related, a least square fit could be made to calculate the temperature from the voltage. Measurements were made at 1, 2, 5, and 10 microamps. Those at the lower end were found to be the most accurate with correlation coefficients generally around .9999.

A test was then run at a nominal ambient temperature of 100°C. Different currents were applied to the heating resistor and temperatures at the diodes sensed. The results of one such test are shown below in Table IV-1. Diodes 1 is 21 microns from the heating element, diode 2 is 16 microns, and diode 3 is 11 microns.

TABLE IV-1
DIODE TEMPERATURES FOR DIFFERENT HEATING CURRENTS

Heating Current (mA)	Diode 1 (°C)	Diode 2 (°C)	Diode 3 (°C)
1	99.09	98.97	98.99
2	99.22	99.15	99.10
5	100.50	100.42	100.40
7.5	102.20	102.17	102.23
10	104.56	104.67	104.81
12	107.69	107.84	107.91
15	111.75	112.00	112.38
17.5	116.57	117.14	117.52

From such data a relationship between the current and temperature can be calculated. From the data in Table IV-1,

$$\text{Temperature (Diode 1)} = .05728I^2 + 99.03$$
$$\text{Temperature (Diode 2)} = .05931I^2 + 98.88$$
$$\text{Temperature (Diode 3)} = .06074I^2 + 98.88$$

Correlation coefficients were about .9996. As anticipated, the higher slope for diode 3 indicates that the temperature is warmer nearer the heat source. The specific numbers from these equations imply a temperature difference of .44°C at 17.5mA over the 5 micron between diode 2 and diode 3 - that is a thermal gradient of .09°C/micron. Similarly, between diode 2 and diode 1 there is a temperature difference of .62°C which amounts to a gradient of .12°C/micron. These calculations compare favorably with the

measurements in Table IV-1. The important numbers in this table are the deltas - e.g., the temperature at 17.5mA minus the temperature at 1mA. The temperature delta for diode 1 is 17.46°C and for diode 3 is 18.53°C. This would suggest a temperature drop of more than 1°C across 10 microns - that is a gradient of more than .1°C/micron. The data from Section II indicated the gradient increased very sharply at the edge of the resistor. Thus, it seems clear that the gradient in the silicon at the edge of the resistor is somewhat higher than .1°C/micron and that the gradient in the aluminum is more than .02°C/micron.

This testing was carried out on 2 other units. The results indicated the calculations above were typical.

The thermal characterization was not carried out for the conductor structure on the other side of the heating element because of the liklihood of the metal thermally shorting the 3 points together.

V. PHYSICAL ANALYSIS

Physical and/or metallurgical features of aluminum conductors are known to contribute to the electromigration behavior. Such items as grain size, crystalline orientation, and amount of copper must be accounted for. Of interest also is the degree to which the actual test speciments conformed to the designed physical structure.

The physical characteristics of the metallization on the electromigration test chip were determined by a variety of techniques. As noted earlier the metallization was sputter deposited and consisted of 0.5 microns of Al (0.5%Cu) and 0.1 microns of TiW on 0.6 of silicon dioxide. The test lines had nominal widths of 5.0, 2.5 and 0.7 microns. An overlayer of SiO_2 was used as an etch mask during dry patterning with CCl_4. The samples that were evaluated had not been electrically stressed.

A test die was etched briefly in buffered HF in order to bring out the grain structure. Optical photographs, Figure V-1, revealed micron-sized

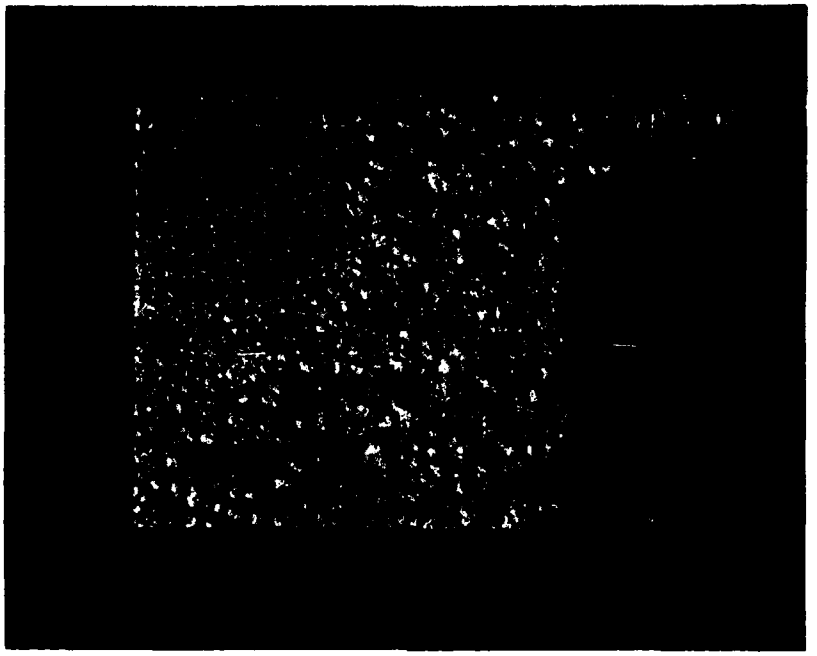

(a)

(b)

Figure V-1. Optical photographs of as-deposited Al(0.5%Cu) test pad that had been etched in buffered HF for two minutes: (a) 450x and (b) 750x.

grains. There was a noticable variation in grain size across the dimensions of a single bonding pad. X-ray diffraction showed that the aluminum had a strong (111) texture, but the Al thickness and Cu concentration were so low that a conventional diffractometer could not detect any second phase.

Samples were thinned for TEM analysis by wet chemical etching and ion milling. The TEM photographs in Figure V-2 indicated a grain size in the 0.3-0.5 micron range. Only aluminum was detected by electron diffraction Figure V-3. Examination of a relatively thick region did not show any distinct Al grains, but there was a fairly uniform distribution of bright spots, Figure V-4, that appeared to be very similar to spots detected in samples of Al (4% Cu) which had been identified as $CuAl_2$ precipitates. The precipitates could also be seen optically, Figure V-5, in samples that had been briefly annealed at 400°C. The precipitates were course and about the same size as the Al grains.

Cross sections of the 2.5 and 0.7 micron lines were prepared and examined in a SEM. The 2.5 micron lines shown in Figure V-6 appeared fairly retangular with dimensions of 2.4 x 0.5 microns as expected. The finest lines seen in Figure V-7 were much more rounded at the corners. It was difficult to determine the actual dimensions from the photographs, but the lines were estimated to be 1.2 x 0.4 microns.

Auger electron spectroscopy (AES) was used to study the distribution of the Cu in the aluminum. The Cu concentration was barely above the detection limit as seen in Figure V-8. The survey was obtained using a large area primary electron beam (excitation source) and high beam current in order to increase the sensitivity. The 5.0 micron lines could not be analyzed using the large area beam since the surrounding Si was always detected. Copper could not be detected with smaller primary electron beams. The bonding pads had large enough areas so they could be depth profiled with the large beam. The low Cu level was not distinguishable from the baseline in a normal profile plot Figure V-9, but it could be determined from the raw data used to generate the

(a)

(b)

Figure V-2. Transmission electron photographs of as-deposited Al(0.5%Cu) metallization: (a) 13,000x and (b) 66,000x.

Figure V-3. Electron diffraction pattern from as-deposited Al(0.5%Cu) taken with 54 mm·Å camera constant. (The photographs are of the same diffraction pattern, but they were developed for different times.)

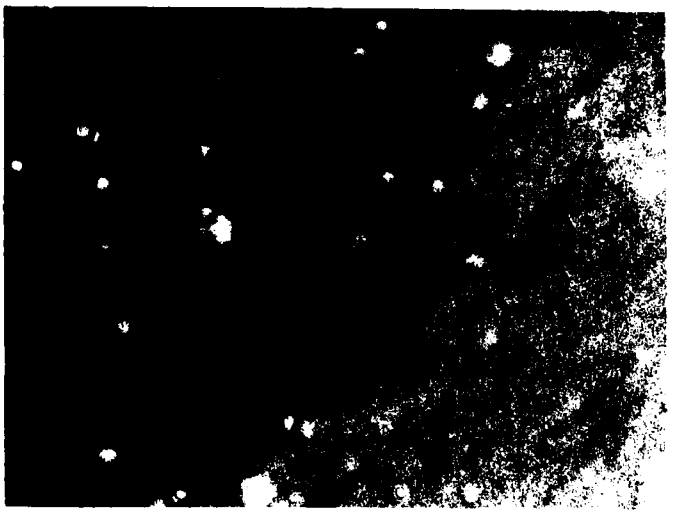

Figure V-4. Transmission electron photograph (50,000x) of a thick region of as-deposited Al(0.5%Cu). The bright spots may be $CuAl_2$ precipitates formed during deposition.

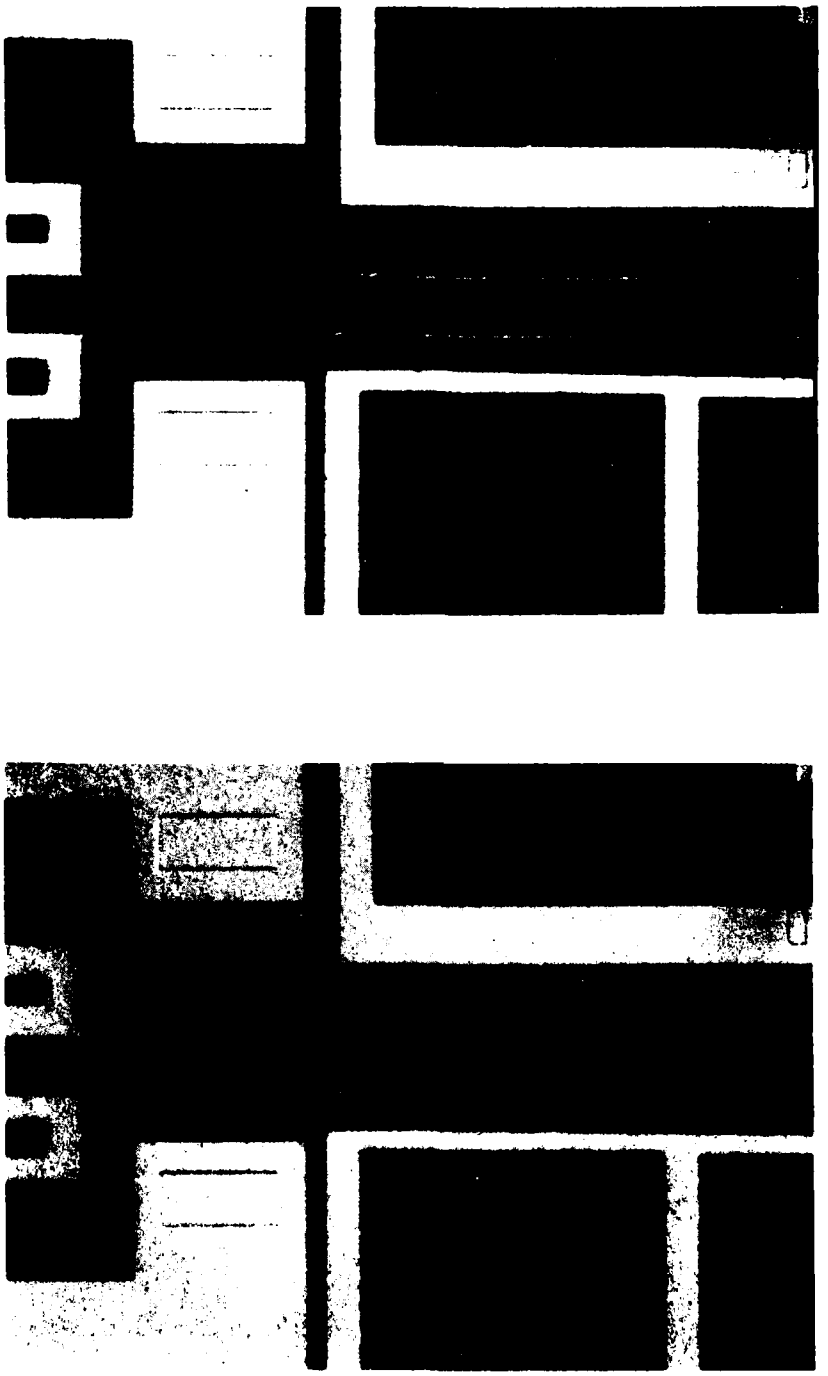

(a)

(b)

Figure V-5. Optical photographs (450x) of 0.7 micron test pattern of Al(0.5%Cu): (a) as-deposited and (b) annealed at 400°C for five minutes. The change in texture was due to the presence of course $CuAl_2$ precipitates.

(a)

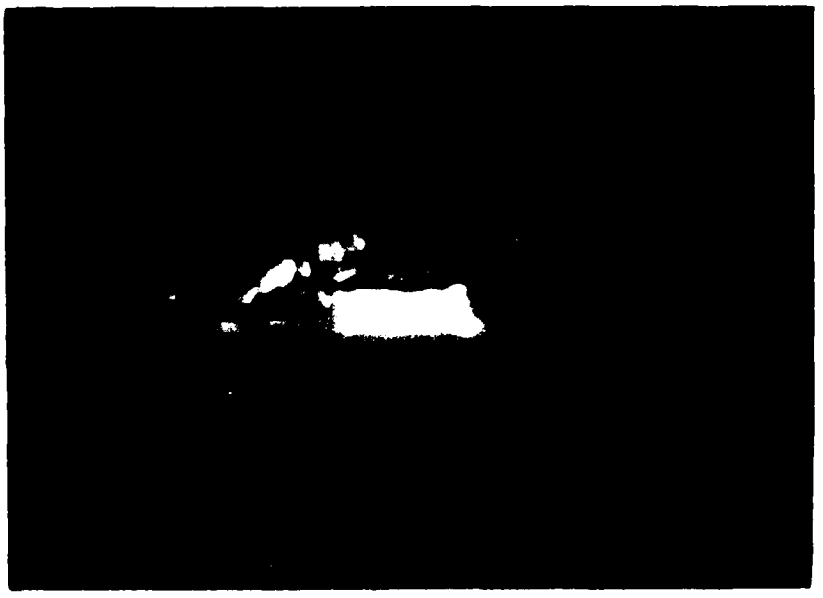

(b)

Figure V-6. Secondary electron photographs of a cross section of an as-deposited Al(0.5%Cu) test line with a nominal width of 2.5 microns: (a) 5,000x and (b) 10,000x.

(a)

(b)

Figure V-7. Secondary electron photographs of a cross section of an as-deposited Al(0.5%Cu) test line with a nominal width of 0.7 microns: (a) 5,000x and (b) 10,000x.

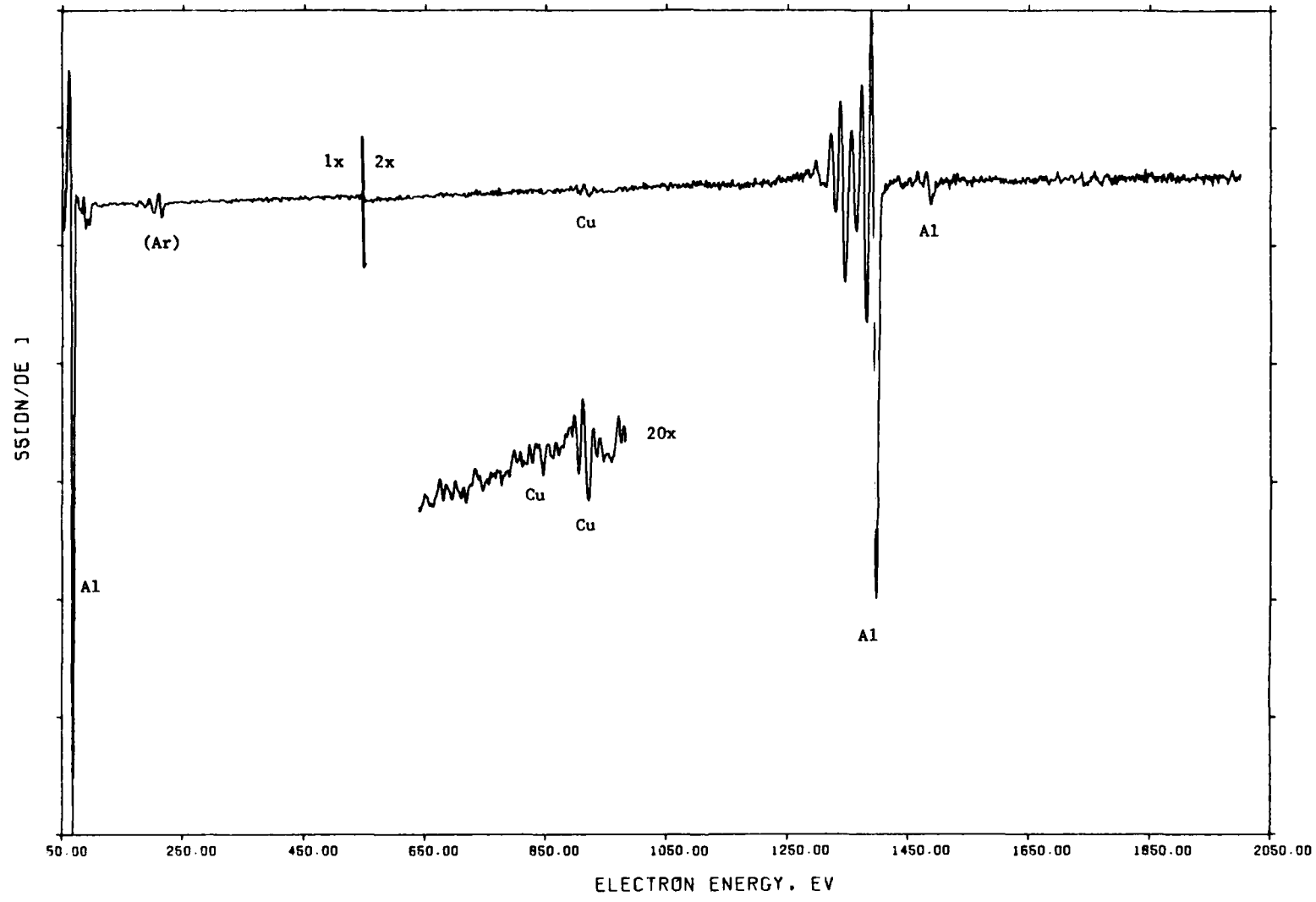

FIGURE V-8
Auger Electron Spectroscopy Survey of Sputter-ion Cleaned Al (0.5% Cu) Bonding Pad.

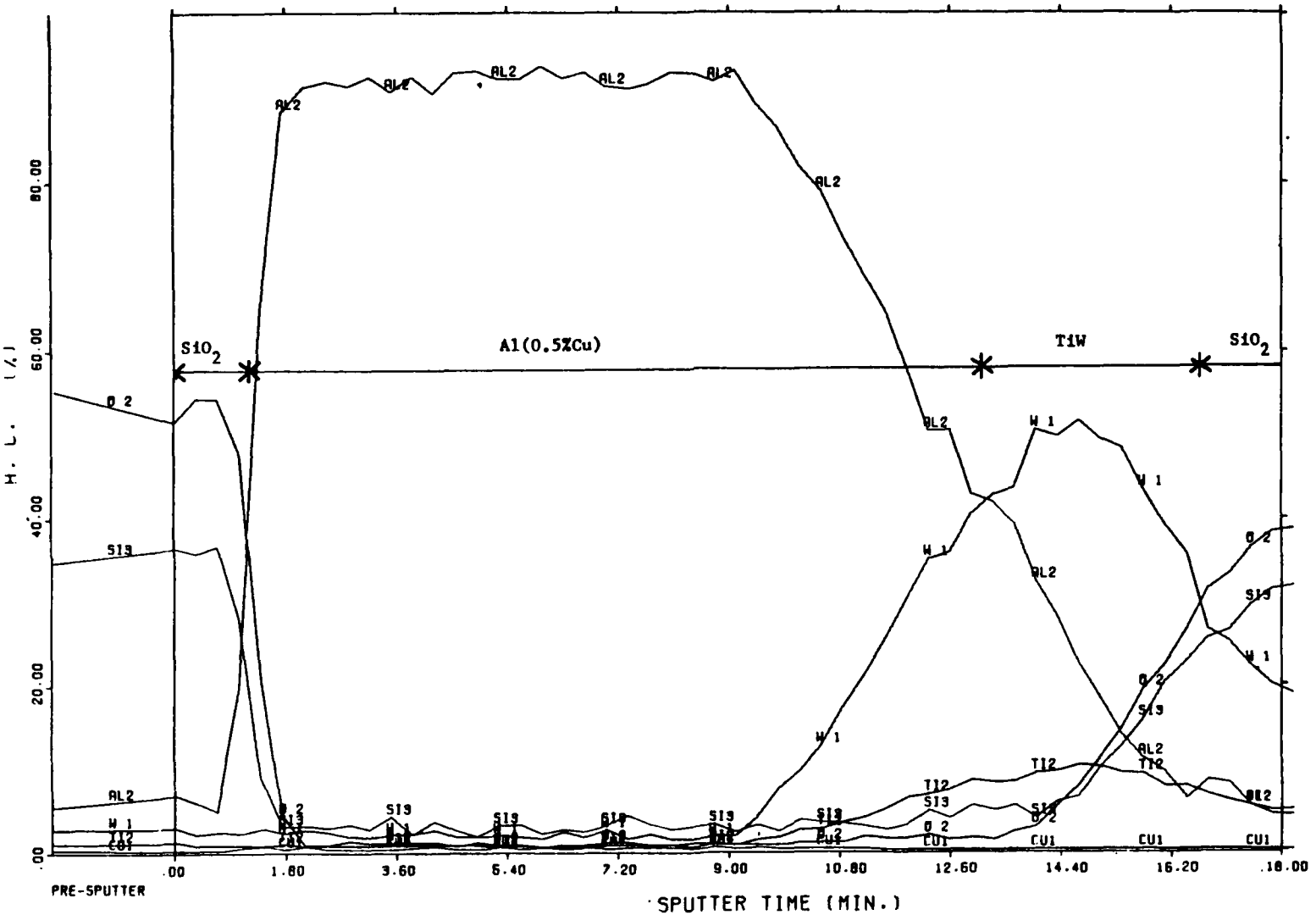

FIGURE V-9
Auger Depth Profile of As-deposited Al (0.5% Cu).
(Sputter Rate ~400Å/Min).

profile. The Cu concentration was calculated to be 0.7 $\pm$ 0.2 atomic percent using sensitivity factors that were not corrected for possible matrix effects. The Cu level was uniform with depth into the aluminum in agreement with previous published studies on sputtered Al (0.5% Cu) thin films. Based on these data, the estimated lateral resolution for AES with the large beam is about 10 microns; and concentration variations of less than 50 percent could not be distinguished readily. Of interest is the fact that the Cu levels were not significant enough for this material to serve as a tracer or marker during the electromigration experiment (it is known that the movement of Cu precedes the movement of aluminum during the electromigration process). It is noted also that the level of silicon in Figure V-9 is a noise level line and does not indicate the presence of a significant amount of silicon.

An electron beam induced current (EBIC) analysis indicated that the edge of the test stripe was lined up with the edge of the implanted resistor (see Figure V-10). This observation was verified by cross sectional analysis. This condition suggests about a 2 micron misalignment. Thus, the thermal gradient experienced by the test conductor will be slightly less than the maximum.

VI. ELECTROMIGRATION LIFETIME TESTING

Thermal modeling by computer has shown that VLSI silicon circuits may produce thermal gradients in the conducting aluminum of more than .1°C/micron. The standard way of determining if such a gradient has an effect on electromigration is thru accelerated life tests -- that is stressing the devices at a higher than normal current and higher than normal temperature until a measureable change is detected. A test vehicle has been designed and fabricated for that purpose.

Because the effect of the gradient could be very suttle, a computerized testing system was configured in which 4 point resistance measurements of each device tested were taken on a regular basis and stored on a magnetic medium. The data could then be manipulated and graphed at a

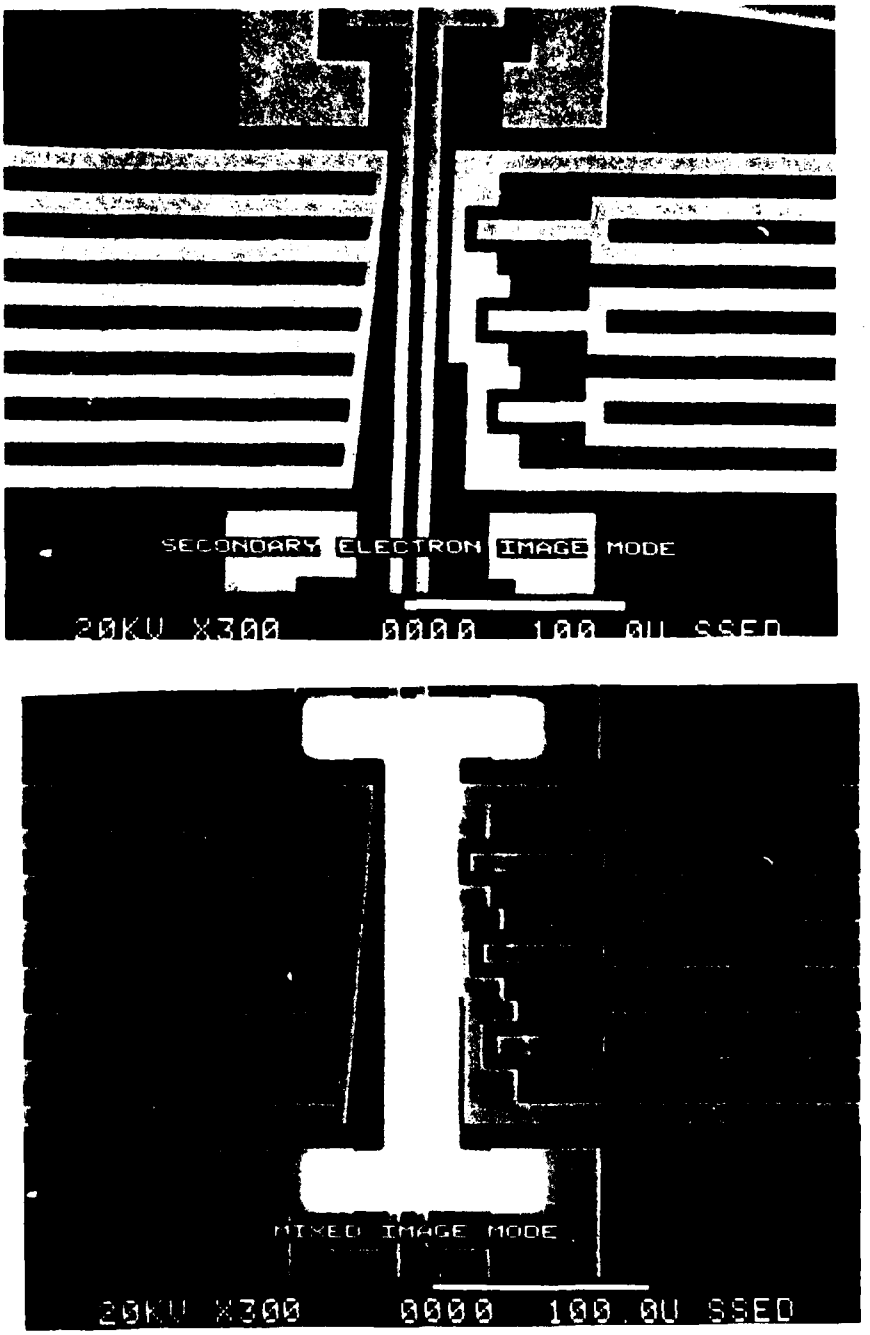

FIGURE V-10

Normal and EBIC Images of Test Device, Showing Location of Diffused Resistor With Respect to Test Stripe

later time, as will be demonstrated later in this section. The data was taken on a Hewlett-Packard 9845B desktop computer using the Image/Query data base system.

In all, four accelerated life tests were run. The fourth, using the submicron lines, was plagued with problems - low yields, failures during test setup and relatively low life times. Its results are not described here. The first 2 tests used 2.5 micron wide lines and the third test used 5.0 micron lines. Each test experimentally compared the electromigration accelerated lifetimes of a set of test stripes exposed to a significant thermal gradient with the lifetimes of a control set of stripes which was stressed at identical conditions except for the lack of a thermal gradient.

The parameters for the first test are described below.

Part No:	3386-8
Test Line Width:	2.5 Microns
Sample Size:	12 with thermal gradient; 12 without thermal gradient (equally split from 2 wafers)
Nominal Resistance:	20 ohms
Thermal Gradient:	Greater than .1°C/u
Ambient Temperature:	150°C
Stripe Temperature	185°C
Current Density:	2.5×10^6 A/cm^2

Each set of parts (i.e., those with thermal gradients and those without) had a separate constant current power supply. Each heating resistor carried slightly more than 17.5mA such that the thermal gradient, beneath the test stripe on the edge of the diffused resistor, was greater than .1°C/micron, per the analysis in the Section IV. The resistance of each test stripe was measured at a low current at 3 different times before the test was started: 1) at 25°C, 2) at 151°C, and 3) at 151°C with the current thru the heater resistor turned on. The first two measurements

allowed a TCR to be established for each individual test stripe. The 3rd measurement, as well as the initial test measurements made at high current, could be used to calculate the average stripe temperature. The resistance, temperature, and time for failure data for the first test are summarized in Table VI-1.

TABLE VI-1

TEST 1: RESISTANCE, TEMPERATURE, AND TIME TO FAIL DATA

Device	OHMS 25°C	OHMS 151°C	HEAT OHMS	HEAT TEMP	TEST OHMS	TEST TEMP	JOULE HEAT	TIME TO FAIL (HOURS)
Center								
101	23.197	32.546	34.525	177.6	35.053	184.7	7.1	105
103	23.825	33.446	35.613	179.3	36.178	186.7	7.3	90
104	23.457	32.976	35.032	178.2	35.711	187.2	8.9	90
105	23.226	32.628	34.639	177.9	35.258	186.2	8.2	145
106	18.289	26.606	28.497	179.6	28.867	185.2	5.6	105
107	23.704	33.272	35.486	180.1	35.999	186.9	6.7	90
108	23.255	32.593	34.635	178.5	35.268	187.0	8.5	125
109	23.677	33.21	35.246	177.9	35.983	187.6	9.7	90
110	23.575	33.053	34.993	176.7	35.788	187.3	10.5	65
111	18.994	27.661	29.892	183.4	30.26	188.7	5.3	45
112	23.447	32.903	35.31	183.0	35.652	187.6	4.5	90
Average	22.6	31.8	33.988	179.3	34.547	186.8	7.5	
Edge								
201	22.321	30.631	32.447	178.5	32.727	182.7	4.2	140
203	23.479	33.029	34.699	173.0	35.466	183.1	10.1	120
204	24.871	34.979	36.814	173.8	37.697	184.8	11.0	90
205	18.568	27.027	28.691	175.7	29.305	182.9	9.1	60
207	18.819	27.411	28.971	173.8	29.572	182.6	8.8	40
208	18.471	26.886	28.434	174.1	29.05	183.4	9.2	140
209	19.54	28.411	30.034	174.0	30.852	185.6	11.6	75
211	23.714	33.304	34.87	171.5	35.795	183.7	12.1	85
Average	21.2	30.2	31.87	174.3	32.558	183.9	9.5	

Because some of the heater currents did not function properly, the test compared the lifetimes of 11 samples with no thermal gradient and 8 samples with thermal gradient. A typical resistance versus time plot is shown in Figure VI-1. Almost all resistances decreased for the first 25-60 hours of the test. Because the pattern of decrease was similar for a number of the test devices, this condition was attributed to changes in the resistor heat. Slight decrease in oven temperature or thin film annealing could also be factors.

For the purpose of comparison, a 5% resistance increase was considered a failure. From past experience this condition was representative of test stripes in which aluminum voiding had nearly crossed the width of the line. Most resistance increases were monotonic and rapid after this level. Using this criterion, times to failure were found for each test stripe, and a least square fit applied for a log normal distribution. The results are summarized below.

	Group 1 (No Gradient)	Group 2 (Gradient)
t50 (hours)	91	87
Sigma	.34	.52

Thus in this test the gradient caused no significant difference. The joule heating in this test was 7-9 degrees which was more than desired.

The second test used similar samples (i.e. 2.5 micronwide lines) and test set up, but made 2 adjustments: 1) the current density was lowered to $2 \times 10^6 A/cm^2$ to minimize the joule heating effect and 2) the resistance of 3 other test stripes for each set of parts (i.e. the center test stripes in the edge test and the edge test stripes in the center test) were monitored as temperature sensors. The resistances and times to failure for this test are summarized in Table VI-2.

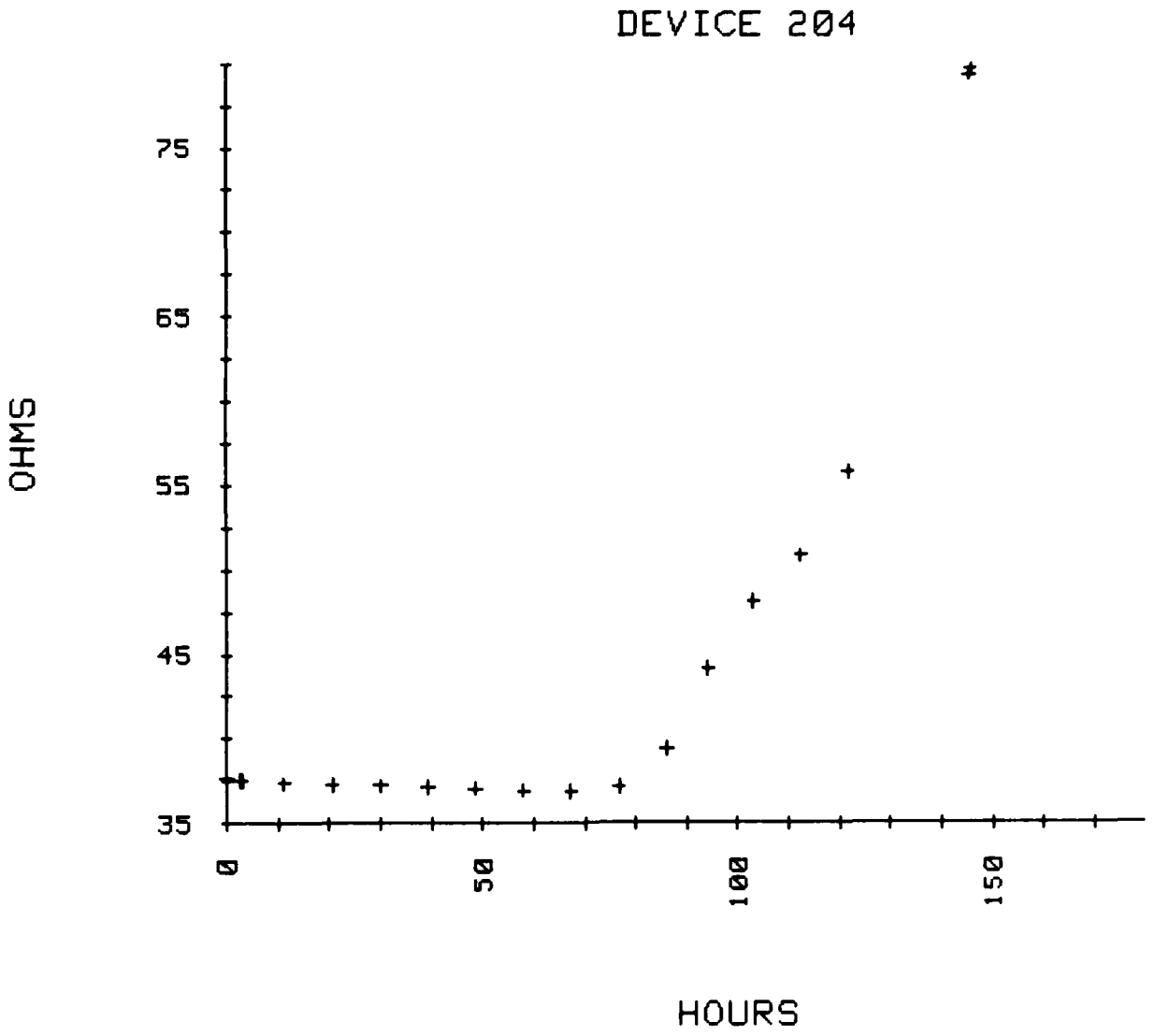

FIGURE VI -1

RESISTANCE VERSUS TIME PLOT OF DEVICE
IN FIRST TEST

TABLE VI-2

TEST 2: RESISTANCE TEMPERATURE AND TIME TO FAIL DATA

DEVICE NO.	25°C OHMS	151°C OHMS	TEST OHMS	TEST TEMP (°C)	TIME TO FAILURE (HOURS)
Edge 101	14.502	20.376	21.136	167.2	320
102	13.477	18.945	19.658	167.4	415
103	13.79	19.408	20.145	167.5	390
104	13.519	19.013	19.752	167.9	365
105	14.027	19.741	20.516	168.0	288
106	13.517	19.013	19.716	167.1	428
107	13.346	18.756	19.475	167.7	---
108	13.753	19.355	20.115	168.0	340
109	13.373	18.828	19.579	168.3	---
110	13.522	18.979	19.724	168.1	410
Average	13.683	19.241	19.981	167.7	
Center 201	13.015	17.891	18.532	167.5	510
202	13.511	18.599	19.693	178.0	---
203	13.419	18.647	19.606	174.0	420
204	13.295	18.486	19.444	174.2	---
205	13.481	18.746	19.764	175.3	265
206	13.492	18.733	19.698	174.1	530
207	13.327	18.513	19.439	173.4	480
208	13.562	18.816	19.791	174.3	485
209	13.469	18.724	19.762	175.8	400
210	13.508	18.766	19.823	176.3	290
211	24.574	18.861	19.915	176.0	320
Average	13.423	18.617	19.587	174.5	

As noted in the previous test, there was a measureable decrease in resistances during the first half of the test. An example of this decrease is shown in Figure VI-2. Since this test stripe had an adjacent test stripe serve as a temperature sensor it was possible to correct the resistance for the decrease in temperature. The temperature corrected resistance is shown in Figure VI-3. All the temperature sensing stripes showed exactly the same characteristic, indicating a systematic temperature drop was taking place. An analysis of this decrease indicated as much as

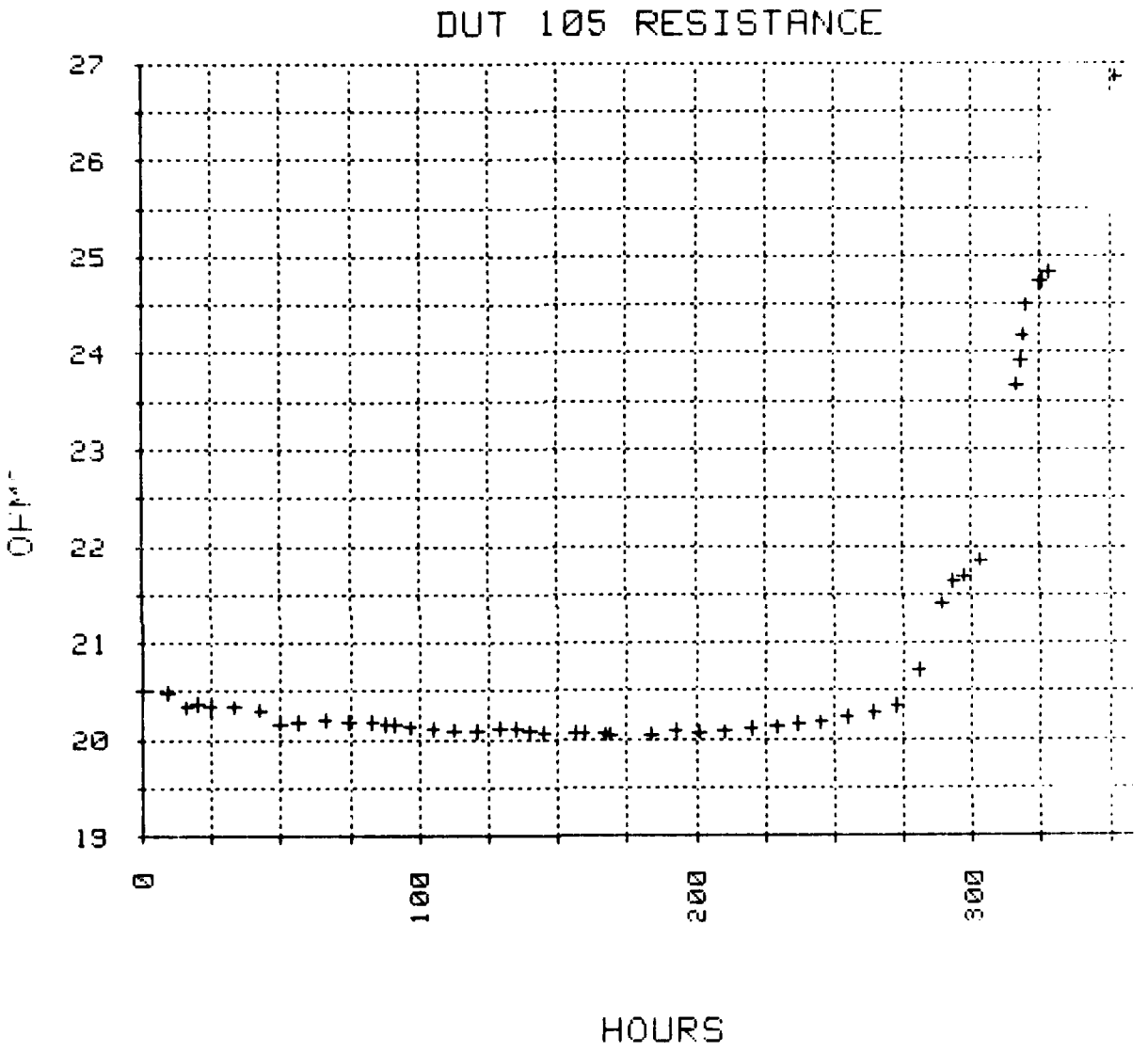

FIGURE VI-2

RESISTANCE VERSUS TIME PLOT OF DEVICE
IN SECOND TEST.

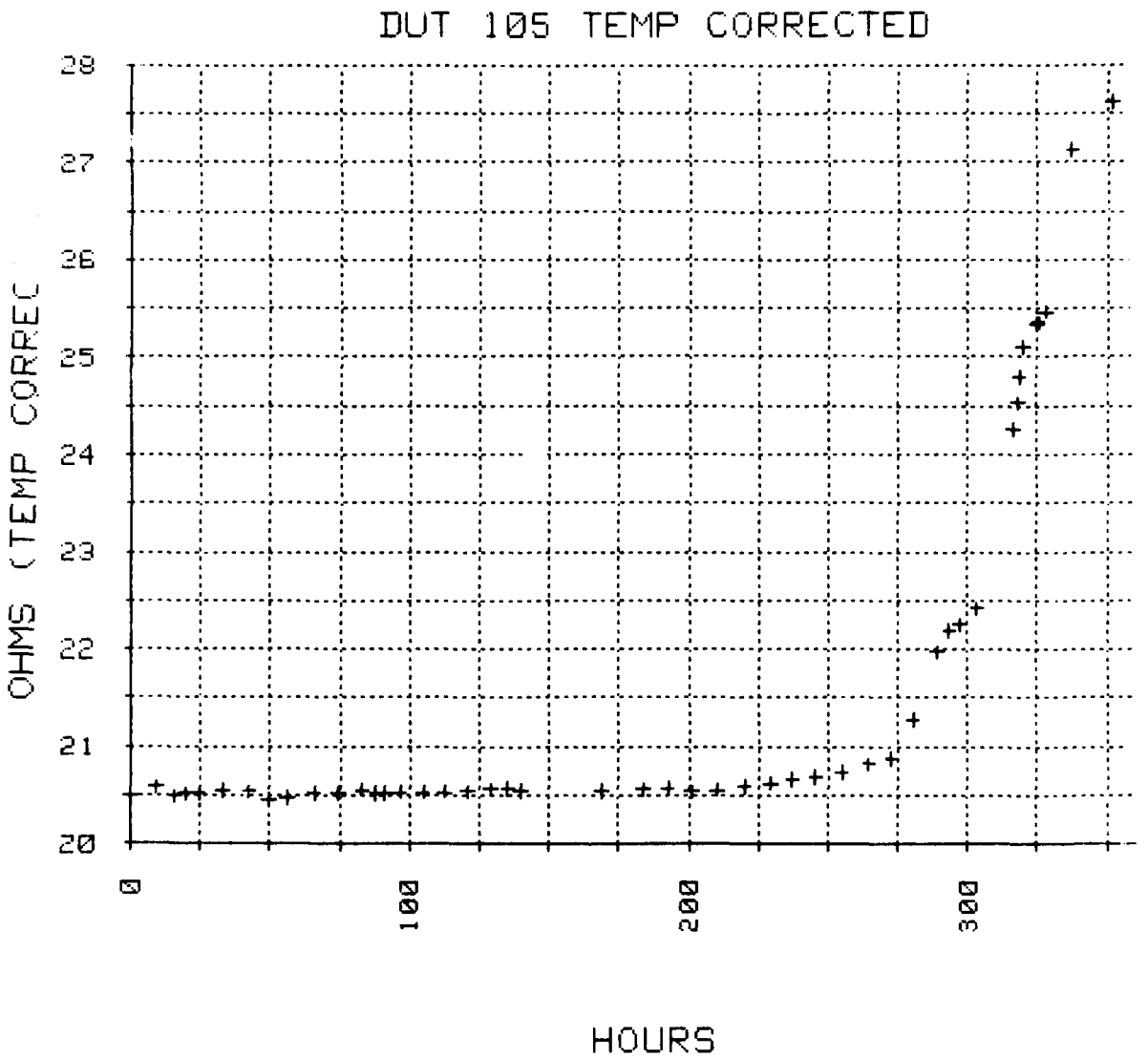

FIGURE VI-3

TEMPERATURE CORRECTED RESISTANCE VERSUS TIME
PLOT OF SAME DEVICE SHOWN IN FIGURE VI-2.

a 10°C drop was slowly occurring over 200 hours. Some 90% of the drop was calculated to be due to decreased heating from the resistor.

With a better understanding of the test stripe resistance changes, times to failure were figured for 2 cases: first, where a 1% resistance increase was considered a failure, and second, where a 5% resistance increase was a failure. Note that the 1% resistance failure time also represents a better measure of the effect of the thermal gradient - the early void growth is important. Later resistance increases might result from hot spots caused by the early voiding, and this condition represents a different thermal picture than the one under study. The results of this work are summarized in Table VI-3.

TABLE VI-3
TEST 2 SUMMARY

	1% Resistance Increase Time to Failure (Hours)	5% Resistance Increase Time to Failure (Hours)
Edge t_{50} Sigma	363 .28	389 .21
Center t_{50} Sigma	398 .32	440 .38

The 3rd test was similar to the second except that the test stripes had 5 micron wide lines. The resistance, temperature and time to failure data from this test are shown in Table VI-4.

TABLE VI-4
TEST 3: RESISTANCE, TEMPERATURE, AND TIME TO FAIL DATA

DEVICE NO.	25°C OHMS	151°C OHMS	TEST OHMS	TEST TEMP (°C)	TIME TO FAILURE (HOURS)
Edge 101	11.323	16.144	17.051	174.1	520
102	11.407	16.242	17.19	175.1	720
103	11.29	16.089	16.998	174.2	650
104	11.242	16.023	16.927	174.2	355
105	11.257	16.061	16.973	174.3	530
106	11.28	16.103	16.99	173.6	775
107	11.179	15.943	16.865	174.7	745
108	11.103	15.824	16.744	174.9	---
109	11.382	16.219	17.177	175.3	380
110	11.477	16.365	17.357	175.9	550
111	11.130	15.875	16.786	174.5	460
112	11.555	16.523	17.449	173.9	580
Average	11.303	16.118	17.042	174.6	
Center 201	11.115	15.516	16.194	169.9	630
202	11.414	16.235	17.016	170.9	650
203	11.257	16.051	16.898	172.7	355
204	11.253	16.039	16.877	172.5	660
205	11.340	16.173	17	172.0	560
206	11.247	16.071	16.913	172.4	540
207	11.431	16.309	17.139	171.9	520
208	11.375	16.205	17.077	173.1	385
210	11.255	16.041	16.982	175.1	---
211	11.148	15.905	167833	173.7	560
212	11.188	15.969	16.783	171.9	---
Average	11.275	16.047	16.878	172.4	

As in the previous test, temperature corrections could be made. The results for this test are shown in Table VI-5.

TABLE VI-5
TEST 3 SUMMARY

	1% Resistance Increase Time to Failure (Hours)	5% Resistance Increase Time to Failure (Hours)
Edge t_{50} Sigma	499 .28	578 .34
Center t_{50} Sigma	471 .25	574 .31

In each test the failures were analyzed. Both optical and scanning electron microscopes were used. Typical failures are shown in Figures VI-4 and VI-5. The horizontal aluminum extrusions or whiskers were not preferentially on one side or the other in either test group (i.e., center or edge). The defect sites were randomly distributed along the line - that is, they had no preference for the positive or negatively biased end. Thus, no effect of crossed thermal gradient was physically observed.

The three tests documented above also measured no effect of a crossed thermal gradient. The second test indicated there may be a 10% lifetime reduction because of the crossed thermal gradient (although the measured effect may be due to the different recorded temperatures shown in Table VI-2). The third test, however, implied a modest lifetime gain for the crossed thermal gradient samples. Thus, no significant difference is evident from the data.

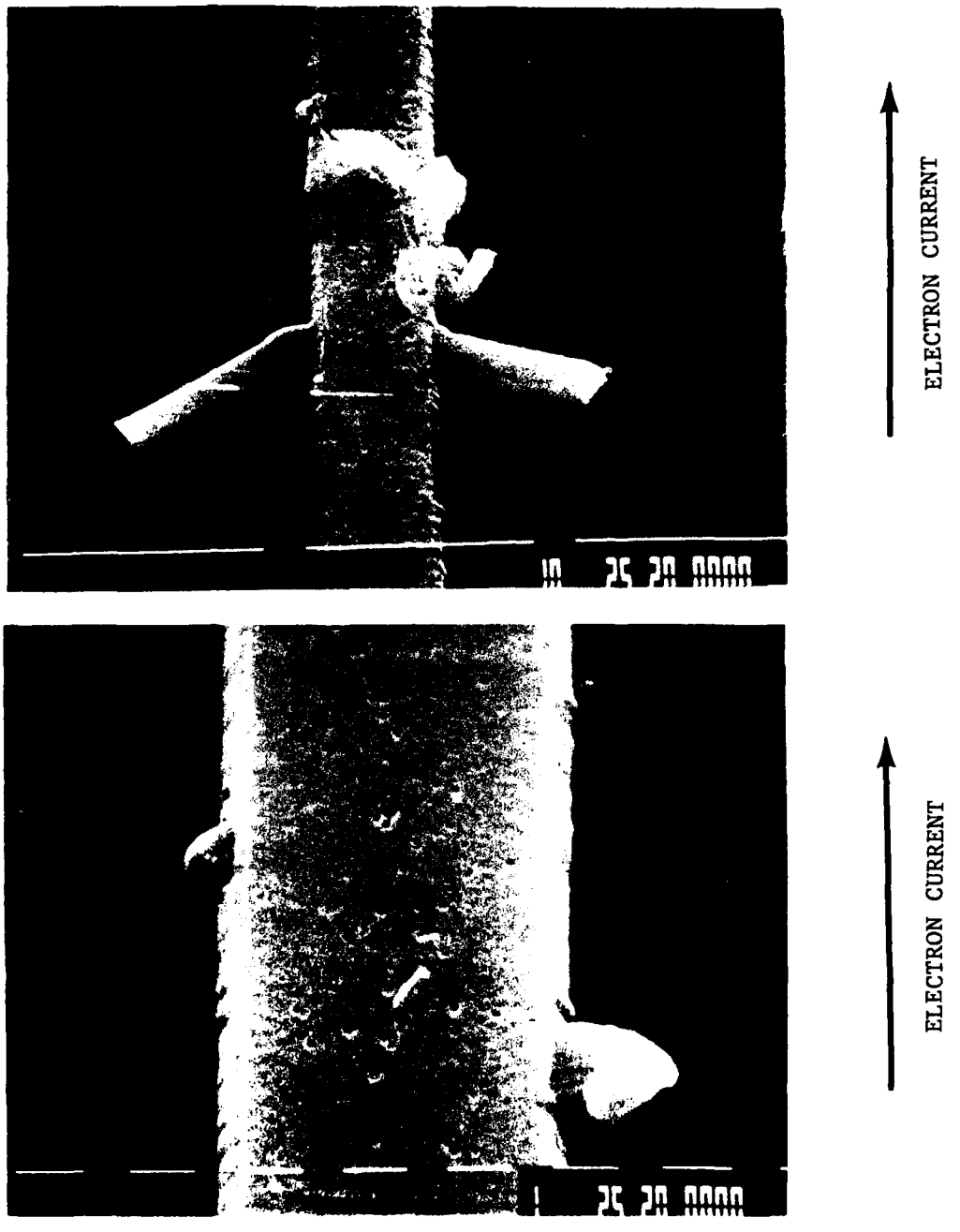

FIGURE VI-4
SEM Pictures of Defects in 5 Micron Lines
Caused by Stress Tests

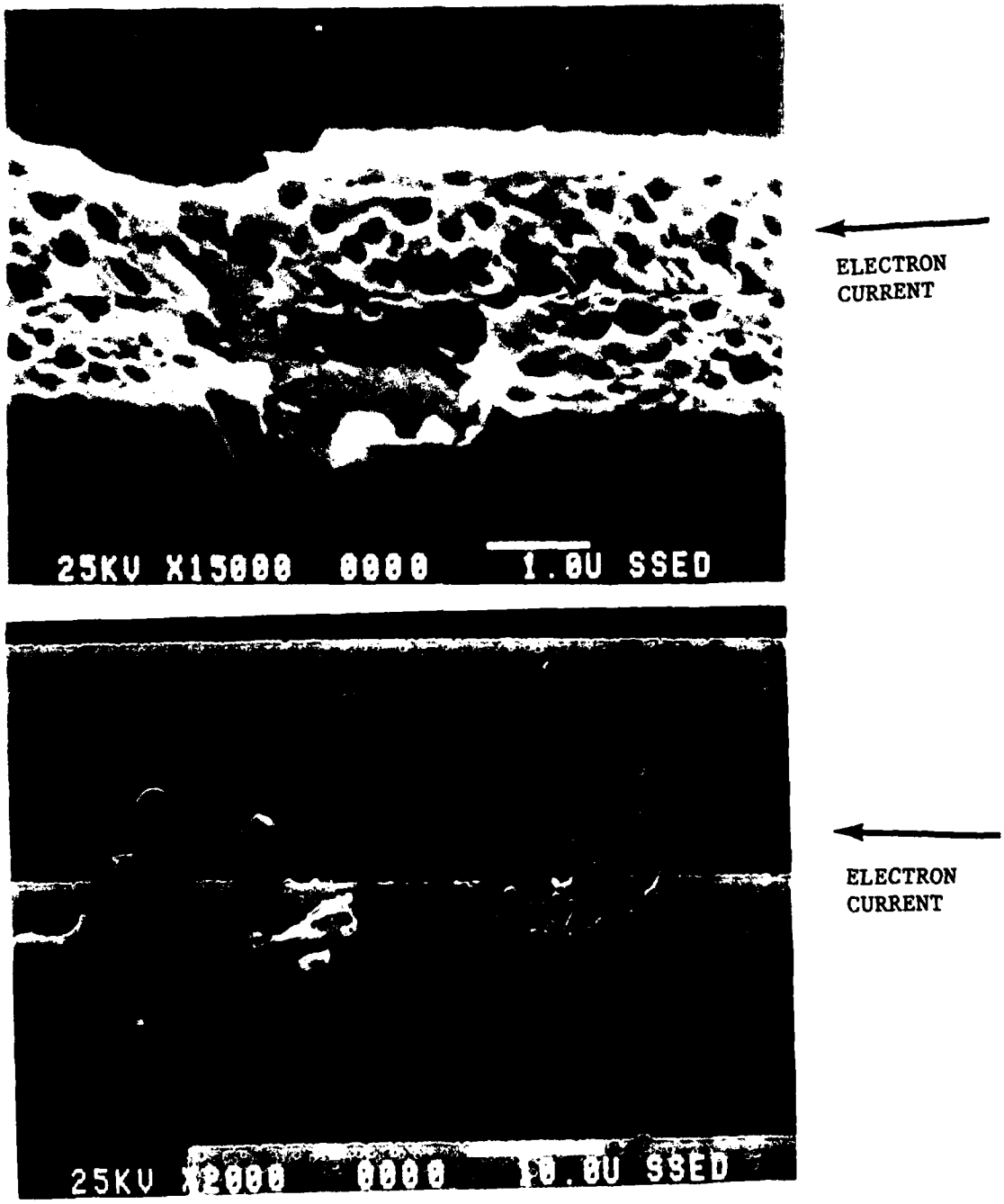

FIGURE VI-5

SEM Pictures of Defects in 5 Micron Lines Causes by Stress Tests.

VII. CONCLUSIONS AND RECOMMENDATIONS

The effect of crossed thermal gradients on the electromigration process was studied and checked experimentally. The gradients on the silicon surface and in the SiO_2 have been shown to exceed .1°C/micron over the edge of a junction. The corresponding gradient in a narrow aluminum conductor above that same junction is somewhat less. The aluminum with its relatively high thermal conductivity essentially shorts out the silicon gradient, but some of this gradient remains.

An experiment was designed to simulate this very situation. The test vehicle utilized an electromigration test stripe parallel to and over the edge of an implanted resistor. The aluminum line on the test site would experience a crossed thermal gradient at least as severe as a real circuit would. Accelerated life tests were run on test stripes experiencing a crossed thermal gradient and similar stripes with the same conditions except no gradient. In three life tests, there was no appreciable difference in the times to failure of the stripes with or without the gradient. There were also no physical signs of this crossed gradient (i.e., hillocks on one side, etc.). Thus, in this experiment no effect of crossed thermal gradient was observed.

The tests were run on 2.5 and 5.0 micron wide lines, but the thermal modeling suggest the results should be applicable to narrower lines.

There are two ways that the gradient on the test samples might have been increased to make the tests even more conclusive. First, the TiW layer should be deleted. This may have had a shorting effect on the gradient in the aluminum. Second, a passivation layer, with as high a thermal conductivity as possible, might be utilized to supply more gradient on the sides and top of the aluminum than the air in the experiment. Any future work along these lines should properly allow for these effects.

The observations reported here are encouraging in that no negative reliability impact is predicted.

MISSION
of
Rome Air Development Center

RADC plans and executes research, development, test and selected acquisition programs in support of Command, Control Communications and Intelligence (C^3I) activities. Technical and engineering support within areas of technical competence is provided to ESD Program Offices (POs) and other ESD elements. The principal technical mission areas are communications, electromagnetic guidance and control, surveillance of ground and aerospace objects, intelligence data collection and handling, information system technology, ionospheric propagation, solid state sciences, microwave physics and electronic reliability, maintainability and compatibility.

END

FILMED

4-84

DTIC